Title page

Assessment of dynamic drought-induced ecosystem risk: integrating time-varying hazard frequency, exposure and vulnerability

Wei Fang[1], Qiang Huang[1], Gordon Huang[2], Bo Ming[1], Quan Quan[1], Pei Li[1], Yi Guo[1], Xudong Zheng[1], Gang Feng[1] and Jian Peng[3, 4]

[1] State Key Laboratory of Eco-hydraulics in Northwest Arid Region of China, School of Water Resources and Hydropower, Xi'an University of Technology, Xi'an, China.

[2] Institute for Energy, Environment and Sustainable Communities, University of Regina, Regina, Saskatchewan, Canada.

[3] Department of Remote Sensing, Helmholtz Centre for Environmental Research−UFZ, Leipzig, Germany.

[4] Remote Sensing Centre for Earth System Research, Leipzig University, Leipzig, Germany.

Corresponding author: Wei Fang (fangwei@xaut.edu.cn), Bo Ming (mingbo@xaut.edu.cn), Quan Quan (qq@xaut.edu.cn)

Highlights

A novel time-varying model is developed to assess drought-induced ecosystem risk.

The proposed model couples time-varying hazard frequency, exposure and vulnerability.

Spatio-temporal variability and driving mechanism of ecosystem risk are elucidated.

The most pressing hotspots where high risk keeps intensifying are identified.

Abstract Terrestrial ecosystems, occupying 28.26% of Earth's surface, are extensively at risk from droughts, which is likely to propagate into human communities owing to loss of vital services. Ecosystem risk also tends to fluctuate within anthropogenically-forced nonstationary environments, raising considerable concerns about effectiveness of mitigation strategies. This study aims to assess dynamic ecosystem risk induced by droughts and identify risk hotspots. Bivariate nonstationary drought frequency was initially derived as a hazard component of risk. By coupling vegetation coverage and biomass quantity, a two-dimensional exposure indicator was developed. Trivariate likelihood of vegetation decline was calculated under arbitrary droughts to intuitively determine ecosystem vulnerability. Ultimately, time-variant drought frequency, exposure and vulnerability were multiplied to derive dynamic ecosystem risk, followed by hotspot and attribution analyses. Risk assessment implemented in the drought-prevalent Pearl River basin (PRB) of China during 1982–2017 showed that meteorological droughts in eastern and western margins, although less frequent, were prolonged and aggravated in contrast to prevalence of less persistent and severe droughts in the middle. In 86.12% of the PRB, ecosystem exposure maintains high levels (0.62). Relatively high vulnerability (>0.5) occurs in water-demanding agroecosystems, exhibiting a northwest-southeast-directed extension. A 0.1-degree risk atlas unveils that high and medium risks occupy 18.96% and 37.99% of the PRB, while risks are magnified in the north. The most pressing hotspots with high risk continuing to escalate reside in the East River and Hongliu River basins. Our results provide knowledge of composition, spatio-temporal variability and driving mechanism of drought-induced ecosystem risk, which will assist in risk-based mitigation prioritization.

Keywords: nonstationarity, dynamic risk, drought, ecosystem health, hotspot analysis

1 Introduction

Climate extremes, lying at the outermost tails of historical distributions, usually arise from the severe alternation of water availability and thermal conditions (Diffenbaugh et al., 2017, Rupp et al., 2022). In response to the occurrence of diverse climate extremes, terrestrial ecosystem functioning, productivity and structure can significantly alter as a direct consequence of the hampered photosynthesis, respiration, transpiration and other essential physiological processes (Fang et al. 2019b; Stocker et al., 2019; Zhang et al. 2023). In this way, climate extremes tend to amplify the likelihood that ecosystems fail to function properly, thereby creating climate-related ecosystem risks. Among diverse climate extremes that constitute external forcings of ecosystem risk, droughts in conjunction with their consequent adverse effects have been extensively documented (Keen et al. 2022; Teutschbein et al. 2023). Droughts pose risk to terrestrial ecosystems in a way that water deficits disrupt plant metabolism, nutrient mobility and energy production that are indispensable for all living organisms, usually with water content as high as 65~89% (Li, Tong, et al., 2020; Meza et al., 2020). More importantly, drought-induced ecosystem risks are easily transmitted to surrounding human settlements through mismatches between the supply of ecosystem services and human demand during drought, ultimately exacerbating risks to the human communities closely interrelated (Munns Jr et al., 2016). Therefore, it constitutes a high priority to specifically evaluate the drought-related ecosystem risk and identify risk hotspots, as part of efforts to shift drought preparedness from reactive crisis management to proactive risk reduction.

Risk, according to the Intergovernmental Panel on Climate Change (IPCC; Field et al., 2012) and the United Nations Office for Disaster Risk Reduction (UNDRR; Kelman, 2018), is defined as the likelihood over a specific period when the normal functioning of a community or society is severely altered due to hazardous physical events, leading to widespread negative effects. The definition emphasizes the role of causal hazards as the external forcing, and either natural or anthropogenic systems where hazard impact occurs. An ensemble of preceding studies (Bachmair et al., 2017; Quijano et al., 2015; Tsakiris, 2017) are accustomed to utilizing the product of the drought index and consequent impact to estimate drought-related risk. Given the multifaceted nature of droughts, the use of the drought index as a risk component provides sufficient flexibility in integrating different drought characteristics (such as drought frequency, severity and duration; Li, Tong, et al., 2020) as well as information regarding diverse types of droughts (meteorological, hydrological and groundwater droughts; Sharafi et al., 2020; Zhang et al., 2019), which facilitates risk assessment from a comprehensive perspective. The foregoing efforts exemplify the impact-based approaches to risk assessment. As the drought impact archives are typically sector-specific, a distinct advantage of the impact-based approaches is that risk assessment can be targeted towards dealing with particular concerns over ecosystem, economy, society and cultural heritage, which is key to risk managers from different sectors. However, the impact-based approaches are highly dependent upon the historical drought records, and are only applicable to limited regions with good data coverage, such as developed countries with sophisticated disaster communication networks and traditions (Blauhut et al., 2016). To deal with the limitation, accumulated knowledge provides useful insight that hazard impact is jointly determined by how many environmental services, and socioeconomic assets are exposed to hazards as well as the extent to which the system under investigation is vulnerable to hazards (Field et al., 2012). High levels of exposure and vulnerability tend to give rise to great severity of hazard impact upon natural or anthropogenic systems. Thereby, recent studies (Ahmadalipour et al., 2019; Carrão et al., 2016; Koks et al., 2015) more frequently employ exposure and vulnerability as surrogates of hazard impact, in view of the difficulty in access to quantitative information about the documented impact on human communities and ecosystems. An updated risk formula is generated, which is expressed as a product of hazard, exposure and vulnerability at an accelerated pace (Aerts et al., 2018; Byers et al., 2018; Koks et al., 2019). The hazard-exposure-vulnerability (HEV) approach for risk assessment highlights that exposure and vulnerability, following the hazard, become the other two risk determinants originating from the affected systems (Peduzzi et al., 2009). Exposure and vulnerability with multi-dimensional characteristics (usually having environmental, social, and economic dimensions; Angeon & Bates, 2015; Wens et al., 2019) can be evaluated using composite indicators or index-based methods (Balogun & Onokerhoraye, 2022; González Tánago et al., 2016; Hagenlocher et al., 2019), which involve the integration of a large amount of information (such as the biomass quantity, vegetation types and biodiversity from ecosystems, and the demographic structure, education level, socio-economic status and governance capacity from human communities) from systems where negative impacts arise. Weights assigned to each subdimension of exposure or vulnerability are usually determined via the expert survey (Meza et al., 2020) and multiple criteria decision analysis typically including the analytical hierarchy process (Chakraborty & Joshi, 2016) and fuzzy logic methods (Hoque et al., 2021). Data required by the HEV approach can be more easily retrieved from the annual statistical reports available at either national or regional scale, which is considered as a major advantage compared to the impact-based approach. This advantage has largely contributed to the popularity of the HEV approach in risk analysis community.

The main focus of the preceding risk assessment and the subsequent risk management are directed to human communities. Terrestrial ecosystems, which occupy 28.26% of the Earth's surface, are substantially more vulnerable to drought than human settlements with much lower ground cover (0.38% in 2015) and a more sparse distribution (Melchiorri et al., 2018). However, little attention has been paid to terrestrial ecosystems when assessing drought-related risks. Only limited efforts have been made, with a particular focus on agricultural systems (also termed as the agroecosystem; Jia et al., 2012; Zhang et al., 2019) which is a typical representative of an artificial ecosystem designed and managed to yield crops and animal products (Swinton et al., 2007). Case studies on estimating drought-related risk to agroecosystems are mostly conducted within the hazard-exposure-vulnerability framework. Hazard is usually characterized using the occurrence probability of hazardous events at different intensities (Dalezios et al., 2014). Exposure has a close association with the cultivated area, agricultural GDP and rural population depending on agriculture for survival (Liu, You, et al, 2019). Vulnerability is often measured by means of composite indicators (Meza et al., 2020), which involve the fusion of diverse drivers related to susceptibility (prevalence of undernourishment and fertilizer consumption, for instance), coping capacity (impounding capacity of dams and availability of irrigation facilities) and adaptability (crop density adjustment and species shift). An emerging alternative to the index-based method for vulnerability evaluation is the yield loss functions (Jayanthi et al., 2014) which generate a vulnerability curve (Quijano et al., 2015) or loss probability (Leng & Hall, 2019) under drought stress of particular concern. A steep slope of the vulnerability curve or a large possibility of yield loss conditional on drought scenarios, signifies a high level of crop vulnerability. In addition to agroecosystems, forest risk arising from drought stress has caught growing attention (Brèteau-Amores et al., 2019; Marusig et al., 2020; Peters et al., 2021). Increased attention is due to widespread concern that the frequency and severity of droughts are expected to be exacerbated by climate warming (Trenberth et al. 2014; Yuan et al. 2019), which will exacerbate risks to forest ecosystems — an important net carbon sink that is believed to capture approximately 20% of global carbon dioxide (CO_2) emissions each year. However, in addition to the agricultural system and forest, terrestrial ecosystems more broadly comprise grassland, deserts and tundra. Ecosystem services highly valued by humans are not confined to food production and carbon sequestration as usually investigated, but also include climate regulation, water purification, waste decomposition and habitat provision in close association with human physical well-being. At the current stage, knowledge gap still exists regarding the differentiated risk levels across diverse terrestrial ecosystems and risk hotspot atlas at a wide spatial scale.

When individual components of ecosystem risk — the hazard (i.e., drought herein), exposure, or vulnerability — are investigated, their variations over time have been increasingly noticed under the influence of climate change and human intervention (Chen et al., 2019; Gonzalez et al., 2010; Sarhadi et al., 2016). Risk is explicitly expressed as the product of time-dependent risk components, subsequently determining that ecosystem risk tends to be time-varying rather than static in a nonstationary environment. Firstly, recent studies observed non-stationarity in precipitation across Europe (Rahimpour et al., 2016; Vasiliades et al., 2015), East Asia (Noh et al., 2021; Wang, Li, et al., 2015), North America (Ganguli & Coulibaly, 2017), Australia (Rashid

& Beecham, 2019) as well as 40.3% of 11069 global catchments for streamflow (Yang et al., 2021) in the Anthropocene. Under a non-stationary condition, the mean and variance of precipitation and streamflow become time-variant, introducing changes in the location and shape of statistical distributions, respectively (Salas et al., 2018). Given the alteration of precipitation and streamflow distributions, the likelihood of dry day occurrence — graphically expressed as left-tail probability defined in a fixed domain extending from zero to the specified threshold — can change over time accordingly. As a result, the probability of droughts with designated duration and severity of concern — a commonly used measure of the hazard dimension of risk — is expected to evolve through time. Moreover, exposure of ecosystems to drought stress is largely shaped by fractional vegetation cover and biomass quantity. High exposure arises from either a high fraction of vegetation coverage or a large quantity of biomass where strong water demand is essential to maintain the functioning of ecosystems. Thereby, primary drivers of time-varying exposure are found to be human- and climate change-induced alterations in vegetation coverage or biomass amount, examples of which comprise the massive revegetation in the Loess Plateau of China (Li et al., 2017) and accelerated shift from vegetated land surfaces to human settlement under rapid urbanization (Du et al., 2019). With respect to vulnerability, its temporal dynamics can be partially attributed to different life stages of ecosystems, changes in the accessibility of drought mitigation infrastructure and the evolutionary adaptation of ecosystems to frequent water stress. Several cases elucidating diverse controls over vulnerability include the varied ecosystem vulnerability at different life stages owing to the changing water requirements (Li, Tong, et al., 2020), increased vulnerability related to the declining performance of the antiquated irrigation facilities in agroecosystems (Rao et al., 2016), and diminished vulnerability in association with a higher root zone storage capacity and smaller canopy cover as a part of evolutionary drought coping strategies of ecosystems (Singh et al., 2020). Within a context of global change, time-varying risk is easy to occur as long as any one of the risk components evolves through time. For long-time mitigation planning, disregarding the time-varying nature of risk may result in the unknown performance of mitigation systems in the coming decades (Sarhadi et al., 2016). Therefore, assessment of dynamic ecosystem risk, though rarely conducted before, is of growing importance in a changing climate, which assists in distinguishing hotspot ecosystems where timely risk management is urgently required and in updating the long-term proactive strategies to strengthen reliability of mitigation facilities.

In contrast to earlier static risk analyses that focused primarily on human communities, the particular focus of the current study is directed toward analyzing drought-related risk to terrestrial ecosystems and its temporal variability in response to a changing environment. Detailed objectives are to (a) develop a dynamic drought-related ecosystem risk assessment model (DERM) which incorporates time-varying hazard probability, exposure and vulnerability as risk determinants, (b) generate the high-resolution (0.1-degree by 0.1-degree) ecosystem risk map for hotspot identification, and (c) clarify how ecosystem risk evolves over time and the key drivers of medium to high risk. Results of the study may be useful in increasing knowledge about the composition, spatio-temporal patterns as well as driving mechanism of time-varying ecosystem risk under stress of climate extremes, further supporting risk reduction decisions towards high-priority ecosystems and long-term mitigation planning with desirable performance in the future.

2 Study area and data

2.1 Study area

The Pearl River basin (PRB) in China is selected as the study area. The Pearl River, flowing 2,214 km from Yunnan-Kweichow Plateau in the west to the South China Sea in the southeast (Fig. 1(a)–(b)), has a drainage area of 442.1 thousand km^2 in the territory of China. The river is the third longest in China and the second largest river in terms of annual surface runoff up to 338.1 billion m^3. The PRB has tropical and subtropical climates featuring high temperature and heavy precipitation (Fang et al., 2019a). As depicted in Fig. 1(c), the mean annual precipitation generally decreases westward from 2600 to 800 mm. Despite the relative abundance of precipitation in the PRB, spatial heterogeneity, mainly due to geomorphology, marks the existence of many low-precipitation areas. The uneven distribution of precipitation throughout the year is also observed, which is that only half of the annual total is received in autumn, winter and spring. Pronounced spatio-temporal variability in precipitation makes droughts prevail in the PRB (Li, Wang, et al., 2020). Recent droughts include, but are not limited to, a multi□annual drought persisting over six successive dry seasons (2002–2007) in the first decade of the 21st century and the latest record-breaking drought lasting from 2021 winter to 2022 spring, of which the negative and extensive influence upon agricultural production and diverse ecosystem services has been reported by Dai et al. (2020) and Han et al. (2019).

Fig. 1(d) also presents the PRB ecosystem distribution using land cover data from the Resource and Environment Science and Data Center, Chinese Academy of Sciences (https://www.resdc.cn/data.aspx?DATAID=198). Forests, occupying more than half of the study area (61.92%), dominate the PRB ecosystem. Croplands and grasslands also have relatively high spatial coverage of 21.15% and 11.84%, respectively. The rest 5.09% proportion is categorized as urban areas, water bodies and barren land (Table 1).

Table 1 land-cover in the percentage of main types of ecosystems in the PRB

Type	Forest	Cropland	Grassland	City and town	Waterbody	Barren land
Occupancy	61.92%	21.15%	11.84%	3.17%	1.89%	0.03%

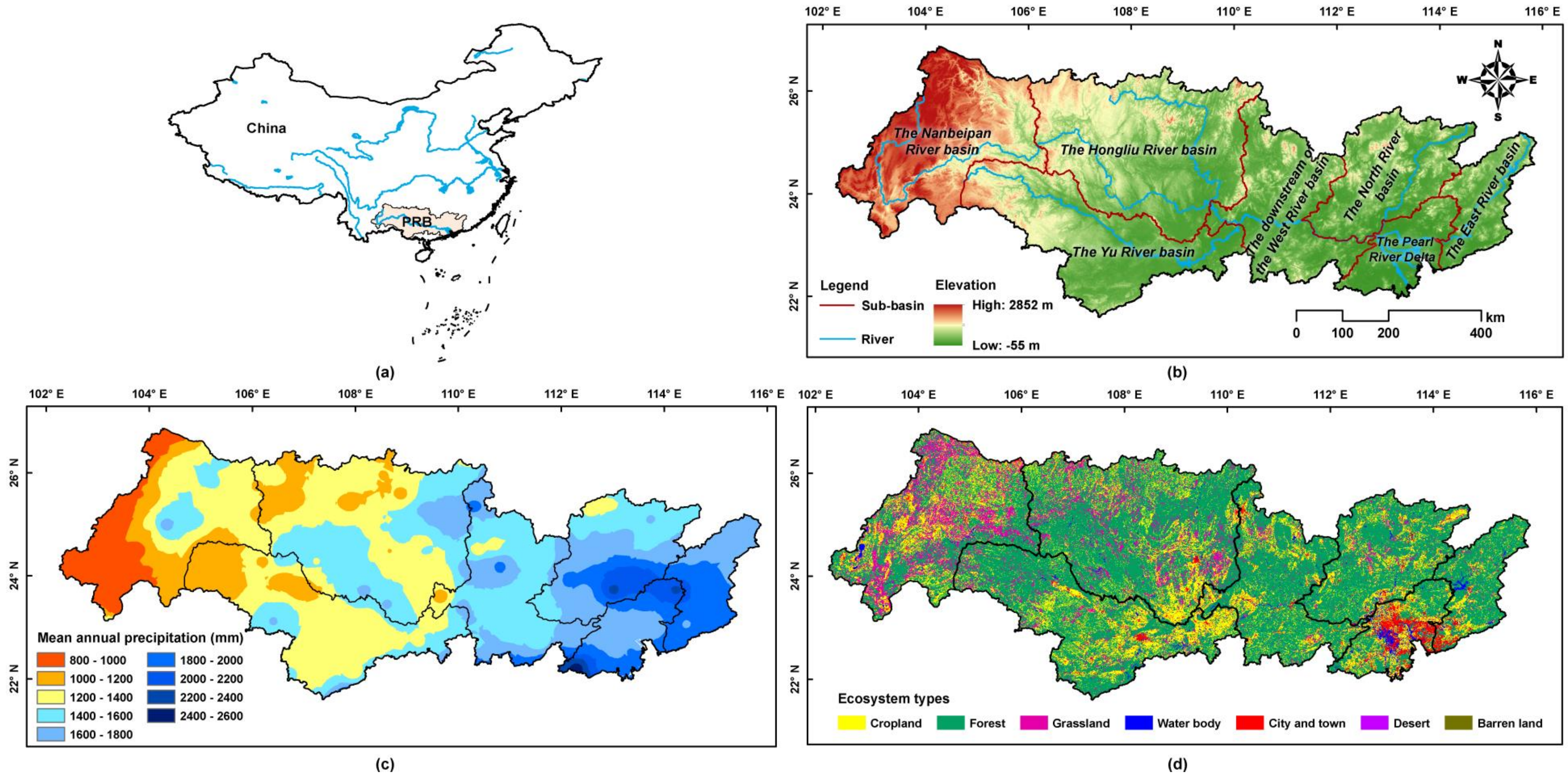

Fig. 1. The PRB location (a), topographic features (b), the spatial pattern of mean annual precipitation (c) and terrestrial ecosystem distribution in the year 2015 (d).

2.2 Data products

Precipitation anomalies are used to identify drought stress as the external forcing of ecosystem risk. Precipitation records are from the China Meteorological Forcing Dataset (CMFD) archived at the National Tibetan Plateau/Third Pole Environment Data Center (http://data.tpdc.ac.cn/en/data/8028b944-daaa-4511-8769-965612652c49/). For the analysis period from 1982 to 2017, the gridded CMFD precipitation has a temporal resolution of 3 hours and a high spatial resolution of 0.1 degree. The CMFD was produced via integrating remote sensing and reanalysis products with ground-based observations at 753 gauging stations affiliated to China Meteorological Administration. The quality of the CMFD precipitation has been verified through intercomparison with rainfall products from the Tropical Rainfall Measuring Mission (TRMM) satellite and the Global Land Data Assimilation System (GLDAS). In the present study, the 3-hour precipitation is aggregated to yield the monthly accumulation, depending on which the Standardized Precipitation Index (SPI) is calculated for monitoring precipitation anomalies over time (Tirivarombo et al., 2018).

Multiple remote sensing products with spatial integrity and temporal continuity are jointly employed for ecosystem exposure and vulnerability assessment, which comprise The Normalized Difference Vegetation Index (NDVI), the Fractional Vegetation Cover (FVC), the Leaf Area Index (LAI) and the Gross Primary Production (GPP) describing terrestrial ecosystem status from different aspects. The NDVI, an indicator for vegetation greenness, is obtained for the same analysis period 1982–2017 from the NOAA's Climate Data Records (CDRs), publicly accessible via https://www.ncei.noaa.gov/data/avhrr-land-normalized-difference-vegetation-index/access/. The NOAA CDRs provide the daily NDVI at a 0.05-degree by 0.05-degreee grid using satellite images captured by Advanced Very High Resolution Radiometer (AVHRR) sensors onboard a series of NOAA polar-orbiting satellites. At present, the AVHRR NDVI dataset is the longest NDVI record available since 1981. Its applicability in the study area has been validated in the preceding studies by Song et al. (2010) and Zhang and Ye (2020). Good agreement on spatial patterns is observed among the AVHRR NDVI and the other two popular counterparts — the MODIS and SPOT-VGT NDVI. In regard to the FVC, LAI and GPP, they separately refer to the areal proportion of land surface occupied by photosynthetic vegetation (Yang et al., 2013), one-half of the total green leaf area per unit ground area (Myneni et al., 1997), and the total quantity of atmospheric carbon dioxide absorbed by plants via photosynthesis (Campbell et al., 2017). The employed FVC, LAI and GPP are all 8-day gridded (0.05-degree by 0.05-degree) products coming from the Global Land Surface Satellite (GLASS, http://www.glass.umd.edu/) product suite developed by Liang et al. (2021). Data reliability has been evaluated against in-situ measurements, indicating that the GLASS FVC, LAI and GPP exhibit favorable performance with the R^2 respectively equal to 0.834 (Jia et al., 2019), 0.96 (Li et al., 2018) globally and more than 0.5 at over 95% of the studied sites (Zheng et al., 2020). Four types of remote sensing products at either a daily or a 8-day scale are monthly aggregated using the maximum value composite method. Subsequently, the obtained monthly composites at 0.05-degree grids are resampled to 0.1 degree to match the resolution of the gridded CMFD precipitation.

3 Methods

Fig. 2 provides an illustrative description of the proposed DERM model for assessing drought-related ecosystem risk with time-variant properties in a changing environment. The DERM model consists of four progressive modules — namely, (a) calculation of bivariate nonstationary frequency of drought jointly considering duration and severity, (b) development of a multi-dimensional indicator to estimate vegetation exposure to drought stress, and (c) trivariate probabilistic quantification of ecosystem vulnerability conditioned on drought scenarios (i.e., the pairwise duration and severity), and (d) post analysis for identifying ecosystem risk hotspot, dynamics and main drivers. The constituent modules are sequentially outlined in this section.

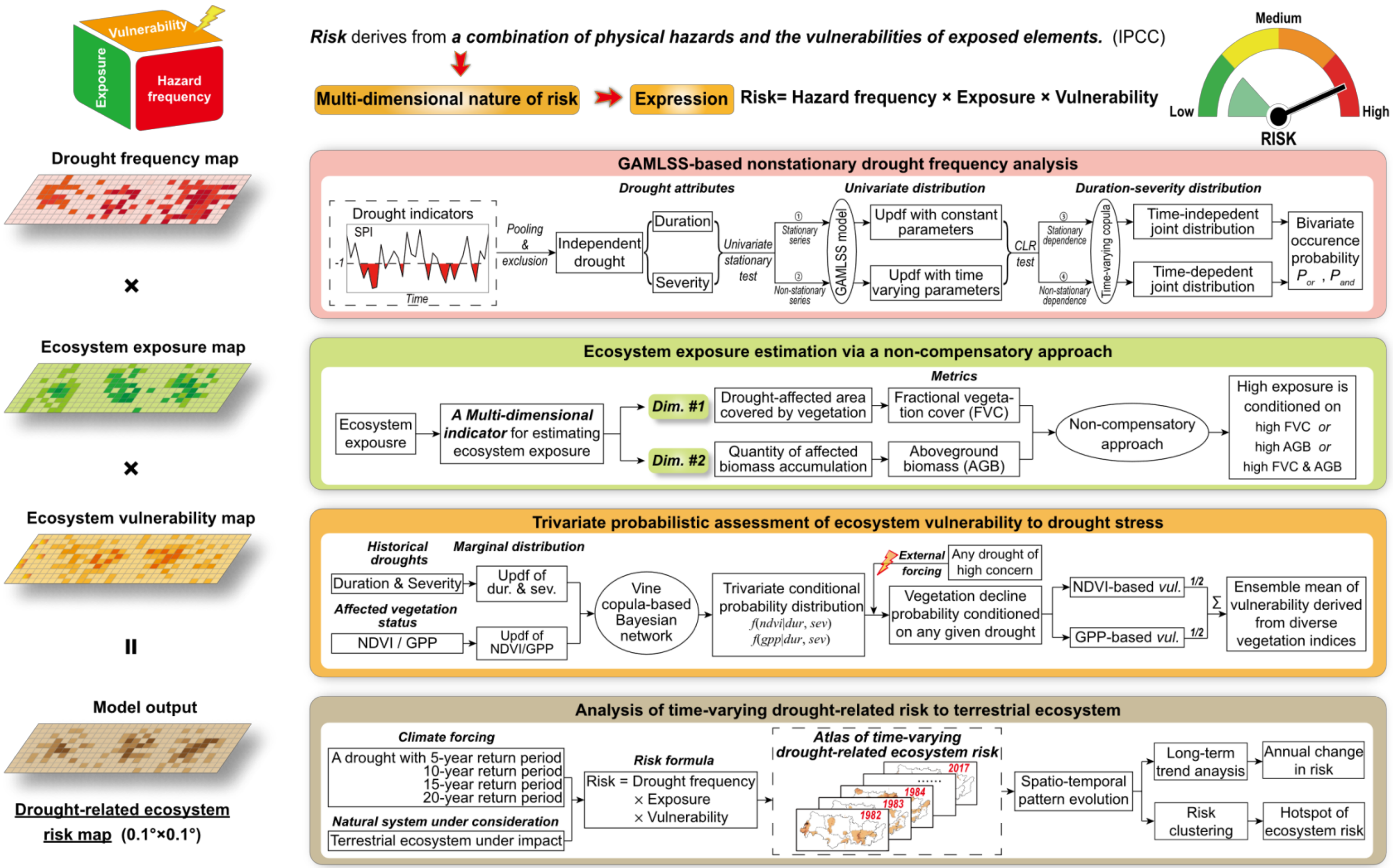

Fig. 2. The schematic of the DERM model integrating three risk determinants for ecosystem risk assessment.

3.1 Bivariate nonstationary drought frequency analysis using a GAMLSS model

3.1.1 Joint use of the truncated SPI and IC method for independent drought identification

In drought frequency analysis, the Standardized Precipitation Index (SPI) is utilized to distinguish water deficits. The SPI recommended by the World Meteorological Organization as a reference drought indicator (Svensson et al., 2017) has received extensive application in the assessment of drought impact on ecosystems (Fang et al., 2019c) and drought-related risk analysis (Strzepek et al., 2010). To calculate the SPI, precipitation data with a minimum timespan of 30 years are initially aggregated at a given accumulative period. The Gamma distribution is subsequently fitted to the composite precipitation series for each calendar month independently. Finally, the SPI — a standard normal statistic — is generated from the probability of precipitation composites via an equiprobability transformation which is an inverse normal function used here. The normalization process above, in essence, establishes a one-to-one correspondence between precipitation observations and the normally-distributed SPI with its value below -1 and greater than 1 separately notifying dry and wet conditions (Fig. 3; Spade et al., 2020). The SPI outperforms diverse drought indices in its low data requirement, relatively simple calculation procedure as well as comparability over time and space. Nonetheless, the utilized index is often criticized for ignoring the influence of high temperature, which tends to induce intense evapotranspiration sufficient to aggravate drought situations (Vicente-Serrano et al., 2010). Interested readers are referred to McKee et al. (1993) and Kumar et al. (2016) for more details about the SPI formulation, merits and limitations.

Specifically, the SPI at a 1-month scale (referred to hereafter as the SPI-1) is employed for distinguishing water deficits in the study. Consecutive periods with the SPI below -1 constitute drought episodes, of which attributes like duration (D) and severity (S), onset and termination time are identified by virtue of run theory (Mesbahzadeh et al., 2020). However, the combined application of the SPI-1 fluctuating at a relatively high frequency and run theory categorized as a truncation level approach is easy to introduce a number of mutually dependent droughts and minor droughts. Mutually dependent droughts, exemplified by Case 2 and Case 3 in Fig. 3, are prolonged droughts split into several smaller spells owing to the SPI temporarily exceeding the threshold for a short time, resulting in the violation of the independence assumption indispensable for the succeeding frequency analysis. To minimize dependence of adjacent droughts, an inter-event time and volume criterion (IC) method (Madsen & Rosbjerg, 1995) is utilized to acquire a sequence of independent droughts. Interested readers are guided to supplementary data for detailed procedure for the IC method.

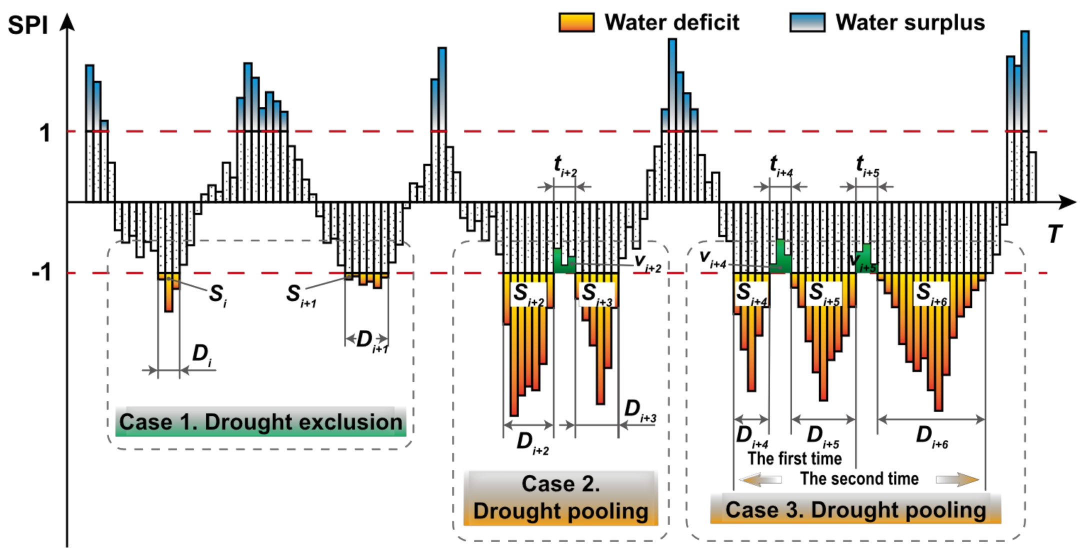

Fig. 3. An illustration of pooling mutually-dependent droughts and excluding minor ones.

3.1.2 Estimation of time-varying bivariate drought probability in a possibly nonstationary context

After independent duration and severity are screened out, the bivariate drought frequency analysis is conducted following four steps.

Step 1. Nonstationarity detection for univariate drought attributes. Nonstationarity in drought attribute series suggests that their mean and variance in close relation with the location and scale of probability distributions change over time. Fig. 4 gives an intuition of nonstationary duration (or severity) having variant exceedance probability q_i as compared to the constant probability in a stationary context, thereby emphasizing the necessity of a nonstationary test towards the accurate estimation of drought frequency. Amid diverse approaches for detecting nonstationarity (e.g., the Mann–Kendall, Spearman, Pettitt and CUSUM tests), the augmented Dickey-Fuller (ADF) test extensively applied in hydrological research is selected mainly due to its specialty in distinguishing the temporal trends in random variables — a major case of violating univariate stationary assumption under climate change (Villarini, Serinaldi, et al., 2009).

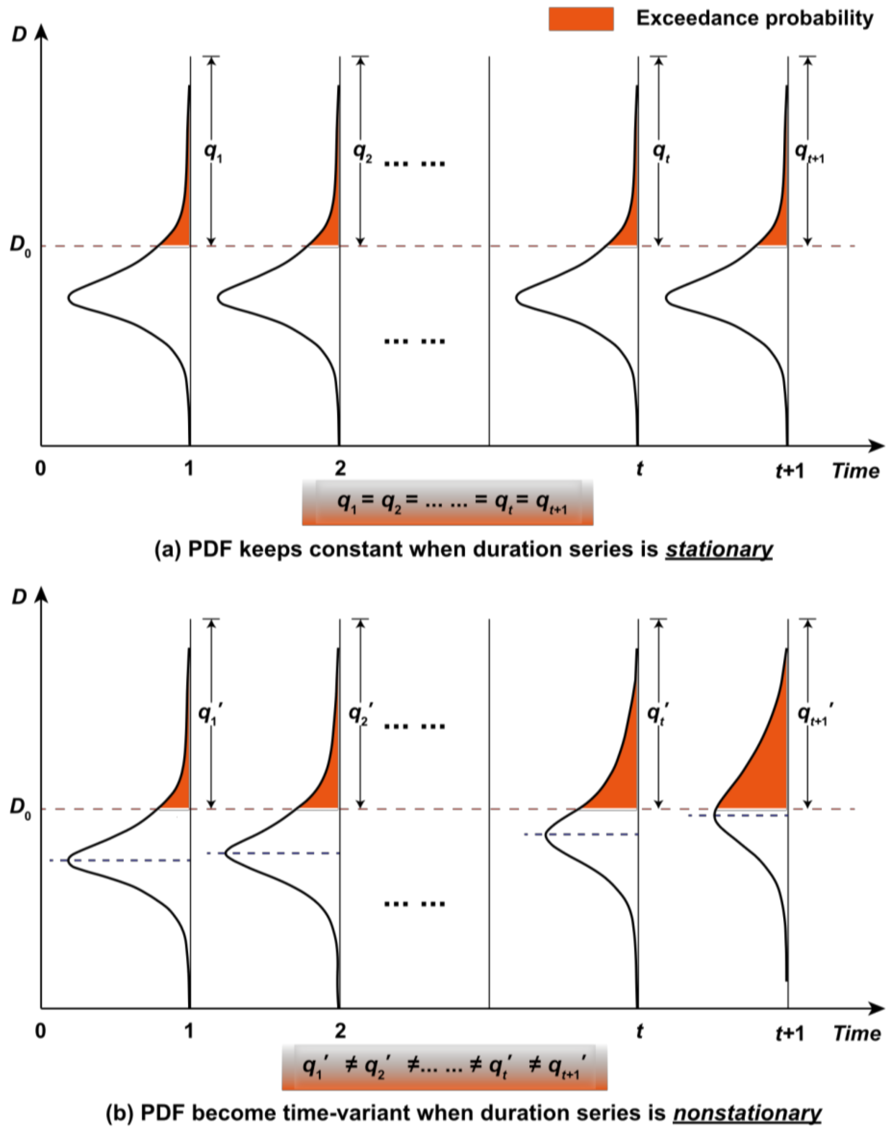

Fig. 4. Time-varying univariate probability (q_t') of exceeding the specified duration (D_0) relative to the constant probability (q_t) in a stationary context.

Step 2. Univariate probability distribution modeling. A total of eight parametric distributions tabulated in Table 2 are fitted to the independent duration and severity series, from which the most appropriate is determined depending on a goodness-of-fit metric — the Schwartz Bayesian Criterion (SBC; Schwarz, 1978) formulated in Eq. (1). The most appropriate candidate having the minimum SBC value is screened out.

$$SBC = GD + \log(n)\cdot df = -2\log L\left(\hat{\mathbf{\Theta}}\right) + \log(n)\cdot df \tag{1}$$

in which GD signifies the global deviance, n is the number of independent observations of duration or severity, df denotes the degree of freedom, $L(\,)$ symbolizes the likelihood function and $\hat{\mathbf{\Theta}}$ is the estimate of distribution parameters.

The key to univariate distribution modeling is how to estimate distribution parameters, especially with time-variant properties under a nonstationary condition. To this end, the generalized additive model for location, scale and shape (GAMLSS; Rigby & Stasinopoulos, 2005) is introduced, providing sufficient flexibility to express distribution parameters as linear or nonlinear functions of explanatory variables and random effects. The GAMLSS model assumes that for $i = 1, 2, \cdots, n$, independent observations of a response variable y_i follow a distribution $f\left(y_i \middle| \mathbf{\Theta}^i\right)$ conditional on $\mathbf{\Theta}^i = \left(\theta_1^i, \theta_2^i, \theta_3^i\right) = \left(\mu^i, \sigma^i, \nu^i\right)$, which is a set of changing parameters determining the distribution location, scale and shape. Relation of distribution parameters with diverse explanatory variables is established via monotonic link functions $g(\,)$ given by Eq. (2).

$$g_k\left(\theta_k\right) = \eta_k = \mathbf{X}_k \beta_k + \sum_{j=1}^{J_k} \mathbf{Z}_{jk} \gamma_{jk} \tag{2}$$

As listed in Table 2, a maximum of three distribution parameters ought to be determined. Eq. (3) is hence detailed as follows.

$$\begin{cases} g_1(\mu) = \eta_1 = \mathbf{X}_1\beta_1 + \sum_{j=1}^{J_1} \mathbf{Z}_{j1}\gamma_{j1} \\ g_2(\sigma) = \eta_2 = \mathbf{X}_2\beta_2 + \sum_{j=1}^{J_2} \mathbf{Z}_{j2}\gamma_{j2} \\ g_3(\nu) = \eta_3 = \mathbf{X}_3\beta_3 + \sum_{j=1}^{J_3} \mathbf{Z}_{j3}\gamma_{j3} \end{cases} \tag{3}$$

where θ_k, μ, σ and ν are distribution parameter vectors of length n, η_k denotes link function values of the equal length n, J_k is the number of explanatory variables introduced as predictors of the k-th distribution parameter, $\mathbf{X}_k$ symbolizes a $n \times J_k$ design matrix consisting of explanatory variables over a total of n time steps, $\beta_k = \left(\beta_k^1, \cdots, \beta_k^{J_k}\right)$ is an unknow parameter vector to be estimated, $\mathbf{Z}_{jk}$ is an already-known design matrix of size $n \times q_{jk}$, and γ_{jk} represents a q_{jk}-dimensional vector composed of random variables.

The present study adopts a semi-parametric additive form of the GAMLSS model (Villarini, Smith, et al., 2009), in which parameters are expressed as cubic spline smoothing functions (i.e., the link function) of time of drought occurrence (i.e., the explanatory variable) to account for their possibly nonlinear variability over time. Other candidate explanatory variables that have potential to explain nonstationarity in droughts can also be applied, and broadly comprise large-scale climate indices and various human disturbances, such as land cover change, water extraction, and reservoir regulations (Das et al., 2020; Jehanzaib et al., 2020; Wang et al., 2020). Time-varying parameters of nonstationary distributions are derived by resolving the model using the Rigby-Stasinopoulos (RS) algorithm to maximize a penalized likelihood (Stasinopoulos & Rigby, 2007). Under a stationary condition, distribution parameters keeping invariant can be estimated using a GAMLSS model as well, only by assigning a constant term to the right side of the link function (Eqs. (2) and (3)). Additionally, it is necessary to note that drought duration and severity always have positive values. Thereby, normal, gumbel and logistic distributions originally defined on $(-\infty, +\infty)$ need to be left-truncated and cumulative probability are revised as Eq. (4).

$$F'(y) = \frac{F(y) - F(0)}{1 - F(0)} = \frac{\int_{-\infty}^{y} f\left(y \middle| \hat{\mathbf{\Theta}}\right) dy - \int_{-\infty}^{0} f\left(y \middle| \hat{\mathbf{\Theta}}\right) dy}{1 - \int_{-\infty}^{0} f\left(y \middle| \hat{\mathbf{\Theta}}\right) dy} \tag{4}$$

in which $f\left(y \middle| \hat{\mathbf{\Theta}}\right)$ is the probability density function (PDF) of a random variable y.

Table 2 Eight types of candidate univariate distributions of drought duration and severity

Name	Expression	Variable domain	Parameter range	Link function
EXP	$f\left(x\middle|\mu\right)=\exp\left(-x\middle|\mu\right)/\mu$	$x\in\Re^{+}$	$\mu\in\Re^{+}$	$g\left(\mu\right)=\ln\left(\mu\right)$
LOGNO	$f\left(x\middle|\mu,\sigma\right)=\exp\left[-\left|\log\left(x\right)-\mu\right|^{2}/2\sigma^{2}\right]\Big/\sqrt{2\pi}\sigma x$	$x\in\Re^{+}$	$\mu\in\Re,\sigma\in\Re^{+}$	$g_1\left(\mu\right)=\mu, g_2\left(\sigma\right)=\ln\left(\sigma\right)$
Gamma	$f\left(x\middle|\mu,\sigma\right)=x^{1/\sigma^{2}-1}\exp\left(-x/\sigma^{2}\mu\right)\Big/\left[\left(\sigma^{2}\mu\right)^{1/\sigma^{2}}\Gamma\left(1/\sigma^{2}\right)\right]$	$x\in\Re^{+}$	$\mu\in\Re^{+},\sigma\in\Re^{+}$	$g_1\left(\mu\right)=\ln\left(\mu\right), g_2\left(\sigma\right)=\ln\left(\sigma\right)$
Weibull	$f\left(x\middle|\mu,\sigma\right)=\sigma x^{\sigma-1}\exp\left[-\left(x/\mu\right)^{\sigma}\right]\Big/\mu^{\sigma}$	$x\in\Re^{+}$	$\mu\in\Re^{+},\sigma\in\Re^{+}$	$g_1\left(\mu\right)=\ln\left(\mu\right), g_2\left(\sigma\right)=\ln\left(\sigma\right)$
Normal	$f\left(x\middle|\mu,\sigma\right)=\exp\left[-\left(x/\mu\right)^{2}/2\sigma^{2}\right]\Big/\sqrt{2\pi}\,\sigma$	$x\in\Re$	$\mu\in\Re,\sigma\in\Re^{+}$	$g_1\left(\mu\right)=\mu, g_2\left(\sigma\right)=\ln\left(\sigma\right)$
Gumbel	$f\left(x\middle|\mu,\sigma\right)=\exp\left\{\left(x-\mu\right)/\sigma-\exp\left[\left(x-\mu\right)/\sigma\right]\right\}\Big/\sigma$	$x\in\Re$	$\mu\in\Re,\sigma\in\Re^{+}$	$g_1\left(\mu\right)=\mu, g_2\left(\sigma\right)=\ln\left(\sigma\right)$
Logistic	$f\left(x\middle|\mu,\sigma\right)=\exp\left[-\left(x-\mu\right)/\sigma\right]\left\{1+\exp\left[-\left(x-\mu\right)/\sigma\right]\right\}^{-2}\Big/\sigma$	$x\in\Re$	$\mu\in\Re,\sigma\in\Re^{+}$	$g_1\left(\mu\right)=\mu, g_2\left(\sigma\right)=\ln\left(\sigma\right)$
GG	$f\left(x\middle|\mu,\sigma,\nu\right)=\left|\nu\right|\theta^{\theta}z^{\theta}\exp\left(-\theta z\right)/\Gamma\left(\theta\right)x$	$x\in\Re^{+}$	$\mu\in\Re^{+},\sigma\in\Re^{+},\nu\in\Re\setminus\{0\}$	$g_1\left(\mu\right)=\ln\left(\mu\right), g_2\left(\sigma\right)=\ln\left(\sigma\right), g_3\left(\nu\right)=\nu$

Note: EXP, LOGNO and GG are abbreviations for exponential, lognormal and generalized Gamma distributions, respectively.

Step 3. Nonstationarity detection for bivariate duration-severity dependence. The consensus about drought as a multi-dimensional phenomenon embedded with diverse attributes (duration, severity, intensity and affected area), has led to a rising propensity to include multiple attributes in drought analysis (Amirataee et al., 2020; Kwon & Lall, 2016). In the study, duration and severity are jointly considered, aiming at a more complete characterization of drought situations. Analogous to the univariate case, the presence of nonstationarity in bivariate duration-severity dependence provokes temporal variation in their joint distributions. Therefore, examining possible nonstationarity in duration-severity dependence also serves as an indispensable step in improving the reliability of drought frequency estimation. The copula likelihood ratio-based (CLR) test is chosen for bivariate nonstationarity detection, among alternative approaches including the well-known Mann-Kendall and Spearman's rho type tests for multivariate trend analysis in panel data (Chebana et al., 2013), as well as the Kolmogorov-Smirnov statistic (Gombay & Horváth, 1999) and Cramér–von Mises statistic (Bucchia & Wendler, 2017) for changepoint identification. The use of copula functions favors a simplified way to derive the complicated multivariate distribution, through modeling marginal distributions and multivariate dependence structure sequentially. The CLR test stems from the notion that the type of copula functions in conjunction with different values of their parameters describes the shape (the upper-tail and lower-tail dependence, for instance) and strength of dependence structure, respectively (Xiong et al., 2015). More technical details about the CLR test are provided in the supplementary data section.

Step 4. Joint distribution modeling for drought duration and severity. Marginal distributions of drought duration and severity are connected using copula functions to yield the corresponding joint distribution. To improve the goodness-of-fit (GOF), five types of candidate copula functions listed in Table 3 are prepared. The estimation of copula parameters diverges owing to the challenge posed by nonstationary dependence structure. In the case of nonstationarity identified via the CLR test, bivariate duration-severity distribution evolves and should be modeled using a copula function with changing parameters, which is termed the dynamic copula (Vinnarasi & Dhanya, 2019) or time-varying copula (Jiang et al., 2015). Following the conceptual framework of the GAMLSS model, a link function — a quartic polynomial of time in Eq. (5) — is developed to mimic temporal volatility of copula parameters $\boldsymbol{\theta}^c$.

$$\begin{cases} \text{Nonstationary dependence.} \ g\left(\boldsymbol{\theta}^c\right) = \boldsymbol{\eta} = \beta_0 + \beta_1 t_i + \beta_2 t_i^2 + \beta_3 t_i^3 + \beta_4 t_i^4 \\ \text{Stationary dependence.} \ g\left(\boldsymbol{\theta}^c\right) = \boldsymbol{\eta} = \text{constant} \end{cases} \quad i = 1, \ldots, n \quad (5)$$

where $g(\,)$ is the link function and $\left[\beta_0, \beta_1, \beta_2, \beta_3, \beta_4\right]$ is a set of parameters to be estimated.

The proposed link function is resolved using a two-step inference function for margins (IFM; Favre et al., 2004), with a goal of maximizing the global log-likelihood of the joint distribution expressed in Eq. (6). Given that the maxima of the first two terms at the right side of Eq. (6) have been calculated by separately screening out the most appropriate marginal distributions for duration and severity in Step 2, the goal is subsequently switched to how to maximize the third term closely related to the density function of copula (Eq. (7)).

$$L\left(\boldsymbol{\theta}^D, \boldsymbol{\theta}^S, \boldsymbol{\theta}^c\right) = \sum_{i=1}^{n} \ln\left[f_D\left(D_i \middle| \theta_i^D\right)\right] + \sum_{i=1}^{n} \ln\left[f_S\left(S_i \middle| \theta_i^S\right)\right] + \sum_{i=1}^{n} \ln\left[c\left(u_i^D, u_i^S \middle| \theta_i^c\right)\right] \quad (6)$$

$$\begin{cases} \left[\hat{\beta}_0, \hat{\beta}_1, \hat{\beta}_2, \hat{\beta}_3, \hat{\beta}_4\right] = \arg\max \sum_{i=1}^{n} \ln\left[c\left(u_i^D, u_i^S \middle| \theta_i^c\right)\right] \\ g\left(\theta_i^c\right) = \beta_0 + \beta_1 t_i + \beta_2 t_i^2 + \beta_3 t_i^3 + \beta_4 t_i^4 \end{cases} \tag{7}$$

in which θ^D , θ^S and θ^c separately symbolize parameters concerning the duration distribution, severity distribution and copula function, $f(\,)$ and u denote the PDF and univariate cumulated probability, respectively.

Once a parameter set $\hat{\boldsymbol{\beta}} = \left[\hat{\beta}_0, \hat{\beta}_1, \hat{\beta}_2, \hat{\beta}_3, \hat{\beta}_4\right]$ is determined, they are incorporated into the link function (a quartic polynomial in Eq. (5)) to yield the optimal values of time-varying copula parameters. In the case of stationary dependence structure, the same method for estimating copula parameters can be simply applied. A major difference lies in the configuration of the link function, of which the right side is assumed to be a constant implying a time-invariant bivariate distribution in a stationary context (Eq. (5)). After the calibration of candidate copula functions, the best-fitted one is determined with the lowest value of the Bayesian information criterion. Ultimately, bivariate drought probability is calculated under two scenarios. The first one P_{or} in Eq. (8) represents either duration or severity exceeding the designated threshold at diverse return periods (for instance, 1 in 10 years or 1 in 20 years). The latter P_{and} signifies a more harmful situation when both duration and severity go beyond the specified threshold uniformly. In the succeeding process of risk calculation, the bivariate probability derived is employed as a surrogate variable of the hazard component of risk.

$$\begin{cases} P_{or}\left(d > D_{des} \cup s > S_{des}\right) = 1 - P\left(d < D_{des}, s < S_{des}\right) = 1 - F_{D,S}\left(D_{des}, S_{des}\right) \\ P_{and}\left(d > D_{des} \cap s > S_{des}\right) = 1 - P\left(d < D_{des}\right) - P\left(s < S_{des}\right) + P\left(d < D_{des}, s < S_{des}\right) \\ \qquad = 1 - F_D\left(D_{des}\right) - F_S\left(S_{des}\right) + F_{D,S}\left(D_{des}, S_{des}\right) \end{cases} \tag{8}$$

where $F_D(\,)$ and $F_S(\,)$ are cumulated probability functions of duration and severity, 474 and $F_{D,S}()$ represents the joint cumulative probability.

Table 3 Five types of candidate copula functions for bivariate distribution modeling and the associated link functions

Name	Expression	Generation function	Parameter range	Link function
Gaussian copula	$\Phi_{\Sigma}\left[\Phi^{-1}(u),\Phi^{-1}(v)\right]$	/	$\theta \in \Re$	$g(\theta)=\theta$
Clayton copula	$\left(u^{-\theta}+v^{-\theta}-1\right)^{1/\theta}$	$\left(t^{-\theta}-1\right)/\theta$	$\theta \in [-1,\infty] \setminus \{0\}$	$g(\theta)=\ln(\theta+1)$
Gumbel copula	$\exp\left\{-\left[(-\ln u)^{\theta}+(-\ln v)^{\theta}\right]^{1/\theta}\right\}$	$\left[-\ln(t)\right]^{\theta}$	$\theta \geq 1$	$g(\theta)=\ln(\theta-1)$
Frank copula	$\ln\left[1+\left(e^{-\theta u}-1\right)\left(e^{-\theta v}-1\right)/\left(e^{-\theta}-1\right)\right]/\theta$	$-\ln\left[\left(e^{-\theta t}-1\right)/\left(e^{-\theta}-1\right)\right]$	$\theta \in \Re \setminus \{0\}$	$g(\theta)=\theta$
Joe copula	$1-\left[(1-u)^{\theta}+(1-v)^{\theta}+(1-u)^{\theta}(1-v)^{\theta}\right]^{1/\theta}$	$-\ln\left[1-(1-t)^{\theta}\right]$	$\theta \geq 1$	$g(\theta)=\ln(\theta-1)$

3.2 Ecosystem exposure assessment via a non-compensatory approach

Ecosystem exposure to natural hazards can be understood from a generalized definition proposed by the UNDRR (Field et al., 2012). As compared to exposure of human communities, ecosystem exposure to drought is confined to environmental entities and services in places that could be negatively influenced. As a principal constituent of ecosystems, vegetation accounts for a predominant quantity (70±9%) of water loss in the way of transpiration across the global ecosystems (Fatichi & Pappas, 2017; Quan et al., 2018). Therefore, the areal extent and quantity of terrestrial vegetation, combinedly exerting a central role in determining the degree of water stress in ecosystems when drought episodes emerge, are assumed to become major determinants of ecosystem exposure. In the study, an ecosystem exposure indicator with two sub-dimensions is developed.

Dim. 1. Fractional vegetation cover (FVC). The FVC with value 1 stands for a fully vegetated pixel and 0 for bare ground. The use of the FVC enables the comparison of exposed vegetation in the horizontal direction across different geographic units. A larger FVC value approaching 1 signifies a high level of exposure from the horizontal perspective.

Dim. 2. Biomass density. Given the identical vegetation coverage, ecosystem exposure can still be differentiated depending on diverse vertical structures of vegetation biomes, such as canopy size and species composition. Aboveground biomass (AGB) density is a composite metric of vertical structure of vegetation communities in terms of biomass accumulation, subsequently becoming the second sub-dimension of ecosystem exposure developed in the study. High AGB density tends to result in an elevated level of exposure. However, the difficulty in acquiring a reliable AGB density estimate with desirable temporal and spatial coverage is in the way of its practical application to exposure assessment. To address the limitation, the LAI covering a long timespan and the global extent is introduced as a proxy variable, owing to the close LAI-AGB linkage (Weraduwage et al., 2015) often utilized in the process-based crop (Dong et al., 2020) and statistical (Zhang, Ganguly, et al., 2014) models to simulate the AGB variability. In the formulation of an exposure index, the LAI going from 0 to 10 is rescaled within the range 0–1 following Eq. (9). A large nLAI value close to 1 notifies high exposure when the vertical structure of ecosystems catches our attention as well.

$$nLAI_{i,j} = LAI_{i,j}/10 \tag{9}$$

where $nLAI$ is the range-adjusted LAI, $LAI_{i,j}$ is the LAI in the i-th year at the j-th pixel, and 10 and 0 are upper and lower bound of the LAI values, respectively.

Two sub-dimensions aforementioned are incorporated to yield an exposure indicator using a non-compensatory approach (Eq. (10); Carrão et al., 2016). The non-compensatory approach emphasizes that superiority in one component of the exposure index cannot be counteracted by inferiority in any other component. In this sense, an ecosystem is highly exposed to droughts if at least one sub-dimension is sufficiently large. For instance, the largest exposure is for a completely-vegetated pixel or an observation of the highest biomass density. As noted in Eq. (10), annual FVC and LAI are incorporated to yield the exposure indicator. Ecosystem exposure can thereby fluctuate annually and give rise to time-varying ecosystem risk.

$$Exp_{i,j} = \max\left(FVC_{i,j}, nLAI_{i,j}\right) \tag{10}$$

where $Exp_{i,j}$ is exposure in the i-th year at the j-th pixel.

3.3 Quantitative analysis of ecosystem vulnerability based on trivariate conditional vegetation decline likelihood

Ecosystem vulnerability under drought stress is quantified within a trivariate conditional probabilistic framework, where vegetation decline probability is considered an intuitive metric for the degree of vulnerability. When water deficits occur, a large possibility of consequent vegetation decrease implies that an ecosystem is highly vulnerable. An earlier bivariate probabilistic framework proposed by Fang et al. (2019b, 2019c) is limited to leveraging the vegetation anomaly dependence upon water shortage accumulation over a fixed timespan (quantified by the negative SPI at a designated timescale like 3 or 6 months), whilst being inapplicable to vulnerability assessment considering specific information of realistic drought events (such as duration and severity), which is the external forcing of interest in the current study. To this end, improvements are made with the aid of the canonical vine (C-vine) copula technique. The modified trivariate probabilistic framework depicted in Fig. 2 utilizes vegetation indicators as response variables, and a combination of causal drought duration and severity as the external forcing. In this way, it provides sufficient flexibility to evaluate ecosystem vulnerability to any drought episode of high concern. What's more, the proposed framework has potential to expand into arbitrary dimensional space to evaluate the joint effect of multiple drought attributes, which is particularly suitable as more details about upcoming droughts can be accessible via increasingly skillful forecasting systems.

In the proposed framework, trivariate conditional likelihood of vegetation status deteriorating into the specified range $\left[VI_{lower}, VI_{upper}\right]$ during a drought episode (characterized using the pairwise duration D and severity S) is formulated as follows

$$P\left(VI_{lower} \le vi \le VI_{upper} \middle| d = D, s = S\right) = \int_{VI_{lower}}^{VI_{upper}} f\left(vi \middle| d, s\right) \mathrm{d}vi \tag{11}$$

where vi denotes vegetation indicators including multiple remote sensing products — the NDVI and GPP — sequentially applied for the improved reliability of vulnerability assessment, VI_{lower} is the theoretically lowest values of vegetation indicators which are -1 and 0 for the NDVI and GPP, VI_{upper} represents the deteriorating vegetation status set to be the 50th, 40th, 30th and 20th percentiles of long-term historical observations, and $f\left(vi \middle| d, s\right)$ is the probability density function of vegetation conditional on a given drought episode.

Vegetation decline probability under drought stress can be calculated by integrating the conditioned probability density function over the interval $\left[VI_{lower}, VI_{upper}\right]$ using the Cubature package in the R environment. How to derive the conditional PDF $f\left(vi \middle| d, s\right)$ in Eq. (11) subsequently becomes a key to the successful calculation of conditioned vegetation decline likelihood $P\left(VI_{lower} < vi < VI_{upper} \middle| d = D, s = S\right)$. Whereas, deriving the explicit formula of $f\left(vi \middle| d, s\right)$ is subject to considerable complexity. A feasible approach is to turn to the vine copula technique. Initially, trivariate conditional PDF shown in Eq. (12) is expressed as the ratio of $f\left(vi, d, s\right)$ to $f\left(d, s\right)$. The copula theory further assists in resolving either $f\left(vi, d, s\right)$ or $f\left(d, s\right)$ through multiplying the

572 copula density function by univariate PDFs of individual variables involved. The relevant procedure is detailed in Eqs. (13) and (14). Ultimately, $f\left(vi|d,s\right)$ has an updated form (Eq. (12)) in close association with copula density $c\left[F_D\left(d\right),F_S\left(s\right)\right]$ and $c\left[F_{VI}\left(vi\right),F_D\left(d\right),F_S\left(s\right)\right]$, which can be addressed using the 'BiCopPDF', 'RVineStructureSelect' and 'RVinePDF' functions in the VineCopula package for the R environment.

$$f\left(vi|d,s\right)=\frac{f\left(vi,d,s\right)}{f\left(d,s\right)}=\frac{c\left[F_{VI}\left(vi\right),F_D\left(d\right),F_S\left(s\right)\right]}{c\left[F_D\left(d\right),F_S\left(s\right)\right]}f_{VI}\left(vi\right) \tag{12}$$

$$\begin{cases} f\left(d,s\right)=\dfrac{\partial^2 F\left(d,s\right)}{\partial d\partial s}=\dfrac{\partial^2 C\left[F_D\left(d\right),F_S\left(s\right)\right]}{\partial F_D\left(d\right)\partial F_S\left(s\right)}\cdot\dfrac{\partial F_D\left(d\right)\partial F_S\left(s\right)}{\partial d\partial s} \\ \qquad\qquad =c\left[F_D\left(d\right),F_S\left(s\right)\right]\cdot f_D\left(d\right)f_S\left(s\right) \\ F\left(d,s\right)=C\left[F_D\left(d\right),F_S\left(s\right)\right] \\ c\left[F_D\left(d\right),F_S\left(s\right)\right]=\dfrac{\partial^2 C\left[F_D\left(d\right),F_S\left(s\right)\right]}{\partial F_D\left(d\right)\partial F_S\left(s\right)} \end{cases} \tag{13}$$

$$\begin{cases} f\left(vi,d,s\right)=\dfrac{\partial^3 F\left(vi,d,s\right)}{\partial vi\partial d\partial s}=\dfrac{\partial^3 C\left[F_{VI}\left(vi\right),F_D\left(d\right),F_S\left(s\right)\right]}{\partial F_{VI}\left(vi\right)\partial F_D\left(d\right)\partial F_S\left(s\right)}\cdot\dfrac{\partial F_{VI}\left(vi\right)\partial F_D\left(d\right)\partial F_S\left(s\right)}{\partial vi\partial d\partial s} \\ \qquad\qquad =c\left[F_{VI}\left(vi\right),F_D\left(d\right),F_S\left(s\right)\right]\cdot f_{VI}\left(vi\right)f_D\left(d\right)f_S\left(s\right) \\ F\left(vi,d,s\right)=C\left[F_{VI}\left(vi\right),F_D\left(d\right),F_S\left(s\right)\right] \\ c\left[F_{VI}\left(vi\right),F_D\left(d\right),F_S\left(s\right)\right]=\dfrac{\partial^3 C\left[F_{VI}\left(vi\right),F_D\left(d\right),F_S\left(s\right)\right]}{\partial F_{VI}\left(vi\right)\partial F_D\left(d\right)\partial F_S\left(s\right)} \end{cases} \tag{14}$$

in which $F_{VI}\left(\ \right)$ and $f_{VI}\left(\ \right)$ symbolize the CDF and PDF of vegetation indicators, respectively.

When the NDVI is utilized as a vegetation indicator in Eq. (11), trivariate vegetation loss likelihood can be yielded. As shown in Eq. (15), rescaling of the NDVI-based vegetation loss probability to $\left[0,1\right]$ gives rise to a drought-related ecosystem vulnerability index, of which greater values imply a higher degree of vulnerability. It is worth noting that since trivariate vegetation loss likelihood (Eq. (11)) remains constant throughout the analysis period, the resultant ecosystem vulnerability is time consistent as well.

$$vul_{NDVI} = \frac{P\left(NDVI_{lower} < ndvi < NDVI_{upper} \middle| d = D, s = S\right) - P_{NDVI}^{\min}}{P_{NDVI}^{\max} - P_{NDVI}^{\min}} \quad (15)$$

in which $P_{NDVI}^{\max}$ and $P_{NDVI}^{\min}$ are the maximum and minimum of vegetation decline likelihood across the whole study site, respectively.

Likewise, the GPP, can be sequentially applied in Eqs. (11) and (12) as well. To analyze the influence of possible bias in diverse remote sensing products, intercomparison is conducted between vegetation decline likelihood based on the NDVI and GPP. Furthermore, the ensemble mean of multiple ecosystem vulnerability indices is calculated following Eq. (16) to yield a composite index, for the enhanced reliability of vulnerability assessment.

$$Vul = mean\left(vul_{NDVI}, vul_{GPP}\right) \quad (16)$$

3.4 Risk estimation and a k-means-based clustering approach

According to a risk concept increasingly accepted by the research community (Koks et al., 2019; Scheuer et al., 2021), drought-induced ecosystem risk shown in Eq. (17) is estimated through the multiplication of bivariate drought probability (i.e., the external forcing), ecosystems exposure and vulnerability (i.e., impact-related attributes of the affected systems).

$$R = P_{and} \cdot Exp \cdot Vul \quad (17)$$

Herein, it is noted that the first risk determinant in Eq. (17) is concurrent drought probability (P_{and}) jointly considering drought duration and severity. The reason lies in that concurrent drought scenarios are considered more realistic and impactful relative to the widely-investigated univariate scenarios (exclusively considering univariate duration or severity) and the other form of bivariate scenario P_{or} illustrated in Eq. (8). Meanwhile, ecosystem vulnerability can be uniformly evaluated under the same concurrent drought scenario. In this way, Eq. (17) allows for increased flexibility in estimating ecosystem risk arising from any past major droughts or forthcoming droughts of specific duration and severity.

Clustering analysis is an essential step following risk estimation, in favor of efficient relief employment by differentiating high, medium and low levels of drought-induced ecosystem risk. The derived risk is sorted using a k-means method (Jahangoshai Rezaee et al., 2021). K-means — one of the top ten algorithms in data mining — is an unsupervised classifier quite useful when prior knowledge is absent. In risk clustering analysis, the number K of risk clusters (C_k, $k=1,\cdots,K$) ought to be determined in advance. K cluster centroids (u_k, $k=1,\cdots,K$) are randomly initialized amongst a set of risk samples $R=\{r_1,\cdots,r_n\}$, after which each sample r_i can be assigned to the nearest cluster. Subsequently, centroids u_k are iteratively updated to minimize the intra-cluster variance given in Eq. (18) (Galluccio et al., 2012). The updating procedure performs repeatedly and converges when no change is noted in cluster centroids between two consecutive iterations. Ultimately, to determine the risk levels, all samples are partitioned by measuring the Euclidean distance to the optimal cluster centroids.

Popularity of the k-means is largely attributed to conceptual simplicity and computational scalability. However, its performance is limited to high sensitivity to the proper initialization of cluster centroids as well as difficulty in determining the optimal number of clusters. Interested readers can refer to Zhao et al. (2018) for detailed information concerning diverse variants, superiority and limitations of the k-means.

$$\min E = \sum_{k=1}^{K} \sum_{r_i \in C_k} \left\| r_i - u_k \right\|^2 \tag{18}$$

4 Result analysis

4.1 An overview of meteorological droughts as significant external forcing of ecosystem risk in the PRB

The total number, duration, severity, onset and termination of independent meteorological droughts during 1982–2017 were identified via the combined use of the truncated SPI series and IC method for 0.1-degree by 0.1-degree pixels in the PRB. To facilitate spatial heterogeneity analysis across a wide spatial extent, seven sub-basins (Fig. 1(b)) — namely the Nanbeipan River basin, the Hongliu River basin, the Yu River basin, the downstream of the West River basin, the North River basin, the East River basin and the Pearl River Delta — are localized from west to east following the sub-basin partitioning published by China's Ministry of Water Resources.

Maximum duration and severity were initially screened from a total of 4019 pixels, which are compared with historical observations to ensure the reliability of subsequent risk analysis. During the recent four decades, the most prolonged duration is up to 8.23 months, triggering an interannual drought spanning from summer, autumn to winter in 2009–2010. Spatially, the maximum duration falls within a pixel (25.6–25.7°N, 104.5–104.6°E) in the western PRB, which is under the administration of Panzhou, Kweichow province. Almost at the same time in 2009–2010, an 81.34 km neighboring pixel (25.5–25.6°N, 105.3–105.4°E) in Xingren, Kweichow registered the highest severity amounting to 11.67. Two geographic locations identified here are also confirmed by sources from authorities and public media reporting where the longest period and highest severity of precipitation deficits occurred in the study area during the 2009-2010 extreme drought period (http://www.gov.cn/jrzg/2010-02/24/content_1540612.htm; http://www.cnr.cn/zgzb/wjbkc/zytqy/201012/t20101225_507499790.html). Severe reductions in ecosystem services including the yield loss of 1.6 million tons and a maximum 10.9% decrease in carbon uptake (Li et al., 2019), exemplify some ecological consequences of the 2009-2010 centennial-scale drought sweeping Southwest China, thereby calling our close attention to ecosystem risk arising from persistent water scarcity.

Fig. 5(a) exhibits the spatial pattern of the cumulative number of droughts. Prevalence of droughts is noted in the PRB as the number of occurrences varies from 16 to 39 times, with the mean reaching 26.63 times over the past four decades. In terms of mean drought count in sub-basins, the middle PRB — the Hongliu River, the downstream of West River, the Yu River, the North River basins and the Pearl River Delta — have greater drought numbers of 27.31, 27.28, 27.26, 26.93 and 26.94, respectively. As compared, droughts become less frequent in the western (25.69 times in the Nanbeipan

River basin) and eastern (22.76 times in the East River basin) margins of the PRB. Meanwhile, the long-term average of drought duration and severity over the recent four decades is depicted in Fig. 5(b) and (c), respectively. The eastern (1.38 months for the East River basin) and western PRB margins (1.39 and 1.35 months respectively for the Nanbeipan River and the Hongliu River basins) have comparatively longer mean duration beyond 1.3 months relative to the middle portion with a slightly shorter duration around 1.2 months. Mean severity escalating westwards and eastwards reveals the spatial pattern analogous to that of mean duration. In contrast to the total drought number, mean duration and severity uniformly present inverse spatial patterns. Therefore, the middle PRB is subject to more recurrent drought episodes characterized by shorter duration and alleviated severity, and droughts in the eastern and western margins, though being less frequent, tend to be prolonged and deteriorating.

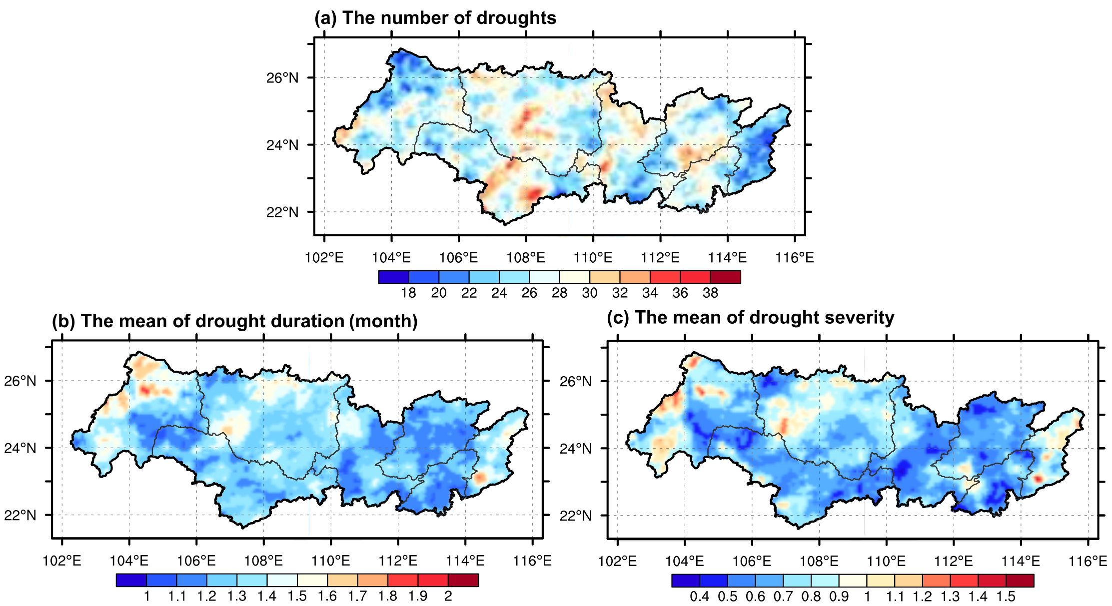

Fig. 5. Drought attributes over the PRB in 1982–2017. (a) The total number of droughts, (b) the mean duration and (c) the mean severity.

The average recurrence interval of 1.36 years reveals the prevalence of drought across the PRB. Except for the rainy summer receiving 46% of the annual precipitation (Liu et al., 2009), there is a high frequency of precipitation deficits in autumn, winter and spring, reaching 37.96%, 35.70% and 39.57% respectively. Autumn droughts are usually the compound consequences of a large proportion of the PRB under control of the western Pacific subtropical high (WPSH) resulting in dry and cloudless days, as well as observably fewer tropical cyclones making landfall in the PRB (Feng & Fu, 2009; Yang et al., 2015). In wintertime, droughts are often attributed to the active cold-dry air intrusion owing to the strengthened East Asian Winter Monsoon in conjunction with a weakening of the northward warm moist airflow from the South Pacific and Indian Ocean (Zhang et al., 2011; Zhang, Zhu, et al., 2014). Spring droughts are highly likely to occur in the wake of winter ones within a year. During spring — a winter-to-summer monsoon transition period, droughts occur under rather different circulation conditions that the weaker Aleutian low and the stronger WPSH jointly provoke more northward convergence of cold and warm airflow out of the PRB domain (Lin et al., 2012).

4.2 Time-variant bivariate exceedance likelihood of droughts in a possibly nonstationary environment

Duration and severity are combined to calculate bivariate drought exceedance probability. Differentiated levels of exceedance probability in favor of distinguishing hazard hotspots are introduced as an ideal surrogate for quantifying the hazard component of risk. According to the risk formula in Eq. (17), a higher probability of exceedance means more frequent drought disturbances. Meanwhile, it is worth noting that to acquire a more accurate outcome of bivariate frequency analysis, potential nonstationarity in either univariate variables (i.e., duration or severity) or bivariate dependence structure are all tested against the stationary assumption. In a nonstationary case, time-varying parametric distributions are prepared to fit drought attributes of concern. Accordingly, the resultant bivariate exceedance probability becomes temporally dynamic rather than static.

Figs. 6–7 exemplify marginal distributions of duration and severity as well as their joint distribution at a pixel (24.6–24.7°N, 105–105.1°E) randomly chosen from the PRB. Results of the ADF test indicate the presence of nonstationarity in univariate duration or severity series, making their probability distributions changeable over time. In such a context, the GAMLSS model is utilized to estimate time-variant parameters of marginal distributions. As seen in Fig. 6, normalized quantile residuals ideally close to the horizontal line in the middle of the worm plot (in essence, a detrended QQ plot), in conjunction with almost all observations located in the scope of a 95% confidence interval, notify satisfactory fitness of the obtained time-varying marginal distributions. Afterward, the joint distribution is developed. Rejection of the null hypothesis proposed in the CLR test firstly helps identify nonstationarity in duration-severity dependence structure at the selected pixel. Bivariate distribution connecting duration and severity is then modeled using a dynamic copula with variant parameters expressed as the quartic polynomials of time. Fig. 7(b) emphasizes that when bivariate nonstationarity is taken into consideration, the derived duration-severity density function achieves the enhanced goodness-of-fit due to the AIC decreasing from -23.39 to -34.65. Across the whole PRB, univariate (duration or severity) and bivariate (duration-severity dependence structure) nonstationarity is detected at 3816 (94.95%) out of a total of 4019 pixels, where temporal evolution of drought exceedance probability is observed.

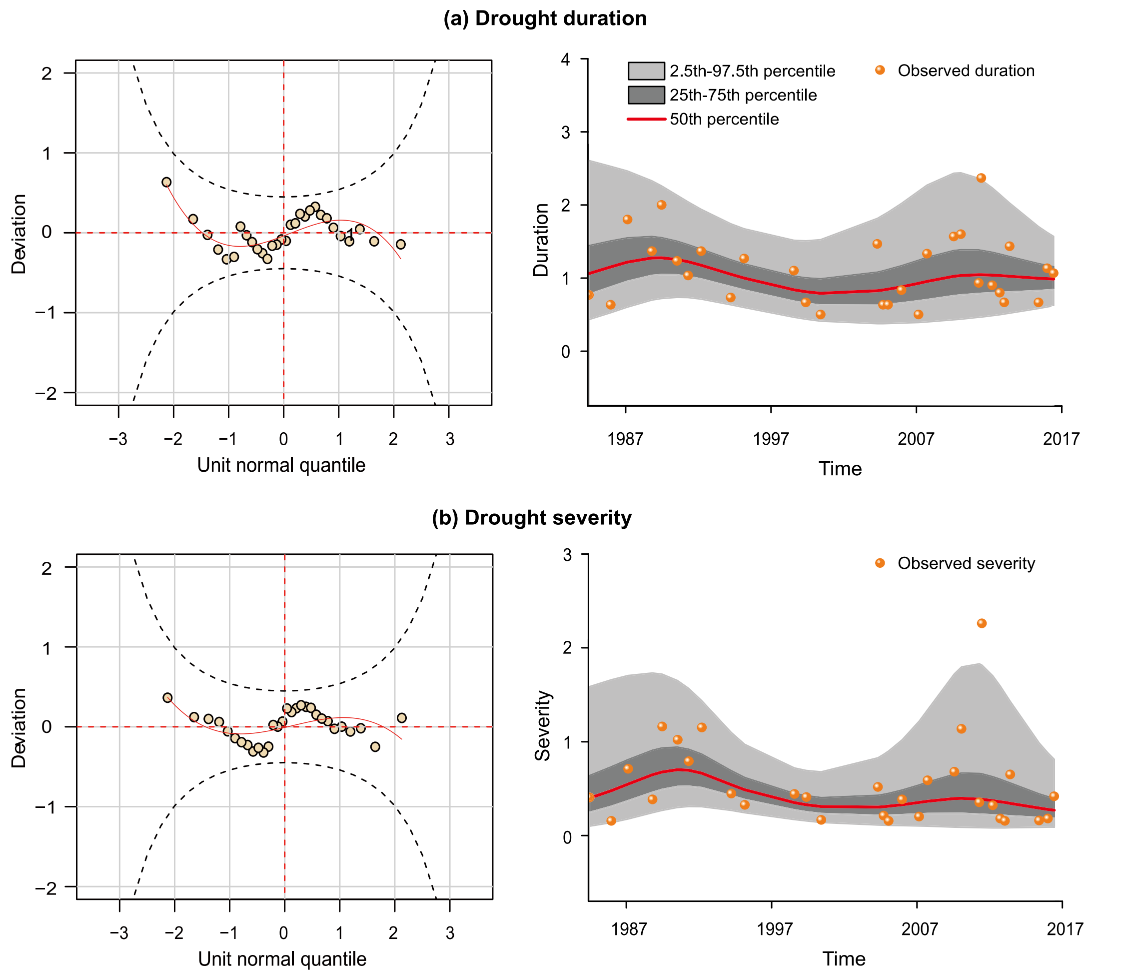

Fig. 6. Worm plots (a) and the time-varying univariate distributions (b) of drought duration and severity at a randomly selected pixel (24.6–24.7°N, 105–105.1°E) in the PRB.

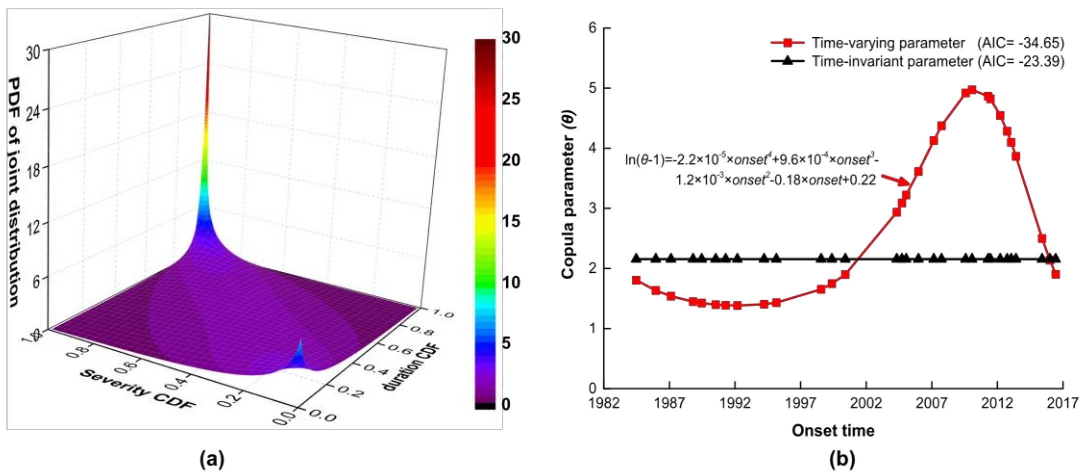

Fig. 7. Probability density of duration-severity distribution derived using dynamic copula function (a) and the time-varying copula parameters (b) in a nonstationary context.

Under two scenarios, bivariate drought exceedance probability is calculated and its mean values over 1982–2017 are depicted in Figs. 8–9. The former scenario (P_{or}) only needs that either duration or severity goes beyond the designated thresholds. In the latter (P_{and}), the requirement of two drought attributes uniformly surpassing the specified values defines a more detrimental scenario. Four sets of duration and severity thresholds are determined with 5-, 10-, 20- and 30-year return periods for the improved reliability of frequency analysis outcome. When designated thresholds escalate from a 5- to 30-year return level, downward trends in drought exceedance probability are shown by an increasing number of dark blue pixels at the bottom-right panels of Figs. 8–9. On a sub-basin scale, an individual panel of Fig. 8 indicates that the NanbeiPan River, the Hongliu River and the East River basins on average have 21.99%, 12.43%, and 20.25% higher exceedance likelihood (P_{or}) relative to the basin mean. By contrast, below-average probability dominates the rest part of the PRB. It is more evident in the east central PRB (i.e., the downstream of the West River basin, the North River basin and the Pearl River Delta) with the mean exceedance probability being -21.30%, -25.57%, and -23.39% lower than the basin average. In terms of P_{and} derived in the latter scenario (Fig. 9), the consistent spatial heterogeneity becomes increasingly pronounced when duration and severity thresholds rise towards a 30-year return level. Both scenarios confirm the vast majority of the east-central PRB are less-probable regions of severe droughts. At a fine 0.1-degree resolution, pixels in color approaching firebrick as an indication of greater exceedance likelihood are scattered over the PRB. As seen in Fig. 8, high-likelihood (P_{or}) patches mainly concentrate in the west of the Nanbeipan River and the west-central Hongliu River basins. Smaller patches are also distributed in the East River basin as well as a transboundary region of the North River basin, the downstream of the West River basin, and the Pearl River Delta. In the case of P_{and} depicted in Fig. 9, almost the identical pixels have a high exceedance probability, except for the transboundary patch as aforementioned. Therefore, bivariate frequency analysis under two scenarios assists in localizing hotspots of influential droughts, which are mainly distributed in the Nanbeipan River basin (especially its western part), the Hongliu River basin (more specifically its west central portion) and a large proportion of the East River basin. As mentioned, dynamic variations of drought exceedance probability emerge at 94.95% of the PRB due to the influence of a nonstationary environment. Mainly located in the eastern Hongliu River and eastern Yu River basins, 1393 pixels (34.65%) favorably witness the descending tendency. However, 2423 pixels (60.28%), mainly located in the remaining five sub-basins, witness an increase in the probability of exceedance.

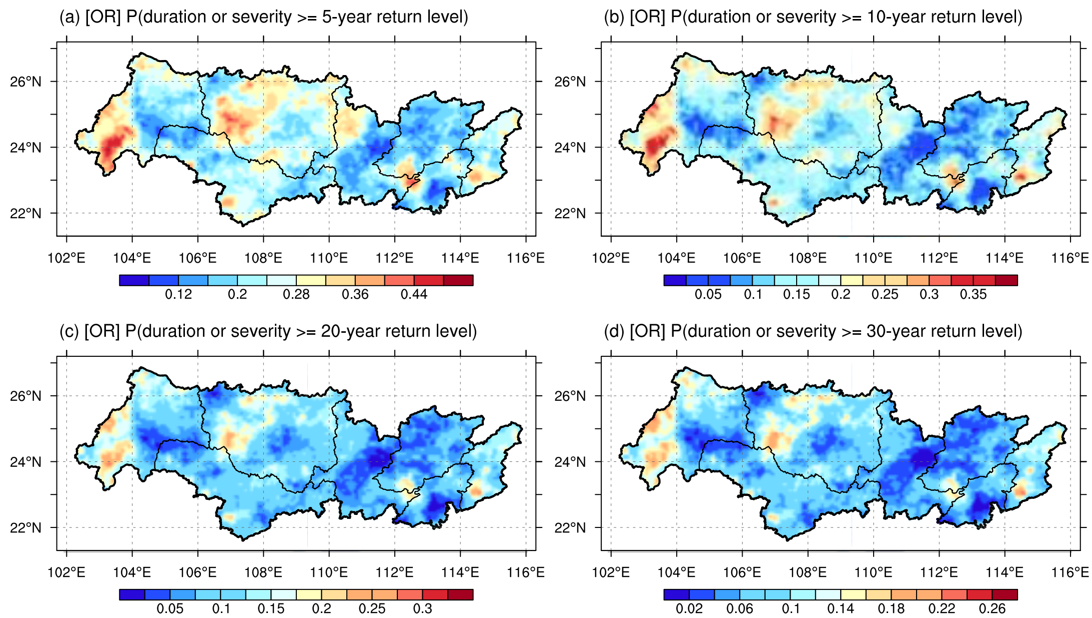

Fig. 8. Mean bivariate probability of exceeding the designated duration or severity ($P_{or}\left(d > D_{des} \text{ or } s > S_{des}\right)$) at (a) 5-year, (b) 10-year, (c) 20-year and (d) 30-year return levels over 1982–2017.

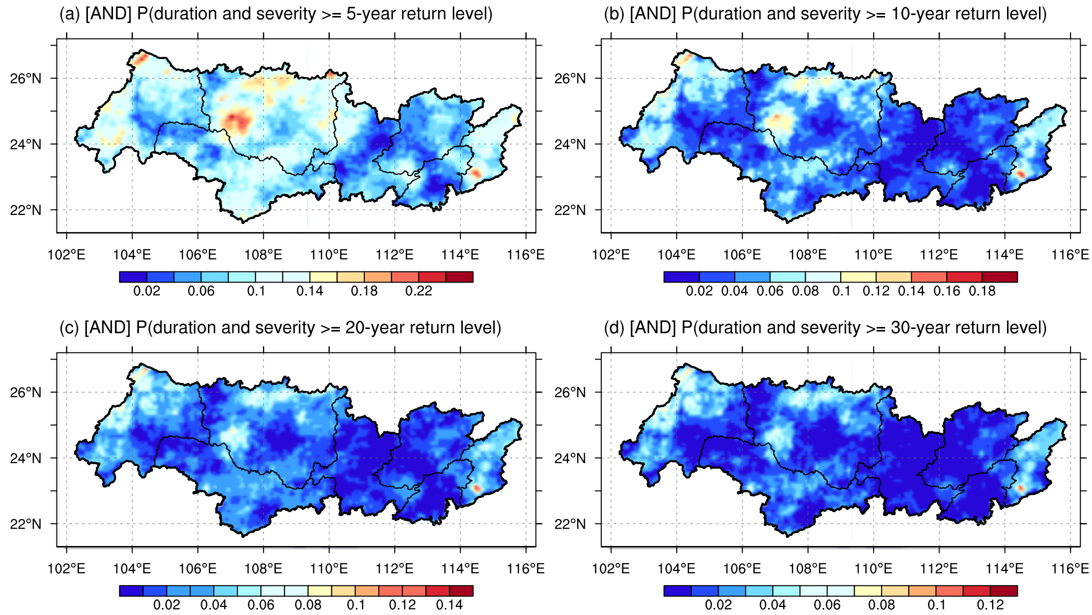

Fig. 9. Mean bivariate probability of concurrently exceeding the designated duration and severity ($P_{and}\left(d > D_{des} \text{ and } s > S_{des}\right)$) at (a) 5-year, (b) 10-year, (c) 20-year and (d) 30-year return levels over 1982–2017.

4.3 Ecosystem exposure and its variations over the recent four decades

A composite index for quantifying ecosystem exposure is formulated in Eq. (10), which takes into account the three-dimensional structure of vegetation biomes. High exposure to drought stress is typically noticed as long as vegetation fraction or aboveground biomass density is sufficiently high. Mean exposure followed by the 1982–2017 variation is shown in Fig. 10.

In Fig. 10(a), the long-term average of ecosystem exposure over 1982–2017 fluctuates between 0.07 and 0.85, with the minimum located at the highly urbanized Pearl River estuary (i.e., the Pearl River Delta) and the maximum in the neighboring East River basin. Mean ecosystem exposure exhibits less profound spatial heterogeneity.

Terrestrial ecosystems have comparably higher exposure across a large proportion of the PRB — more specifically comprising the Hongliu River (0.66), the Yu River (0.64), the downstream of the West River (0.68), the North River (0.68) and the East River basins (0.65) from west to east. However, the Nanbeipan River basin (0.52) in the west and the Pearl River Delta (0.48) at the southeastern margin separately witness the 16.12% and 22.58% decline of ecosystem exposure in relation to the basin average (0.62). It is inferred that a low level of exposure is largely the result of elevation influence upon ecosystem structure in the Nanbeipan River basin within the Yunnan-Kweichow Plateau (1000–2000 m). The high□elevation plateau receives less precipitation and lower temperature, being responsible for the comparatively sparse vegetation with horizontal coverage being roughly 20% below the basin mean. The substitution of grassland for evergreen forests observed at many pixels in the Nanbeipan River basin (Fig. 1(b); Wang et al., 2021) also reminds less biomass accumulation is exposed to drought stress along the vertical direction. Concerning the densely populated and economically developed Pearl River Delta, the observation of even smaller exposure is attributed to intense human activity — especially rapid urbanization. Terrestrial ecosystems reshaped by urbanization have markedly lower vegetation occupation (Liu, Zhan, et al, 2019). Likewise, low exposure owing to urbanization impact is evident in Nanning, Liuzhou and other cities throughout the PRB, as the corresponding pixels marked by circles are in color approaching dark brown (Fig. 10(a)). In addition, the role of agricultural practices — the other type of significant human intervention — in diminishing ecosystem exposure is noticed in the southmost Hongliu River basin and the eastern Yu River basin where the most cropland is located (Fig. 1(d)). Thereby, the above analysis is insightful in understanding the modulation of exposure spatial patterns by intense human activity and elevation.

In addition, over 1982–2017, there exists a slight upsurge of the basin mean exposure estimated to be 2.86%. At a 0.1-degree resolution, the highest growth rate of up to 30.42% is at a pixel of the Nanbeipan River basin. As illustrated in Fig. 10(b), exposure tends to amplify at different rates in the majority (86.12%) PRB covering 3461 pixels. A more marked increase is found in the eastern Nanbeipan River and the Yu River basins, which coincide well with where surface vegetation restoration has been introduced by policymakers as an effective way to prevent karst rocky desertification in Yunnan, Guangxi and Kweichow provinces since 2001 (Wang, Wang, et al., 2015). The downward trend in exposure is recorded at 558 pixels merely accounting for 13.88% of the PRB. The decline in exposure was more dramatic in the central Pearl River Delta, where the largest decline rate (-25.41%) was also recorded. According to previous studies (Du et al., 2020; Liu et al., 2022), this is due to rapid urban expansion leading to fragmentation of ecosystems, reduction in vegetation area and exposure to drought stress.

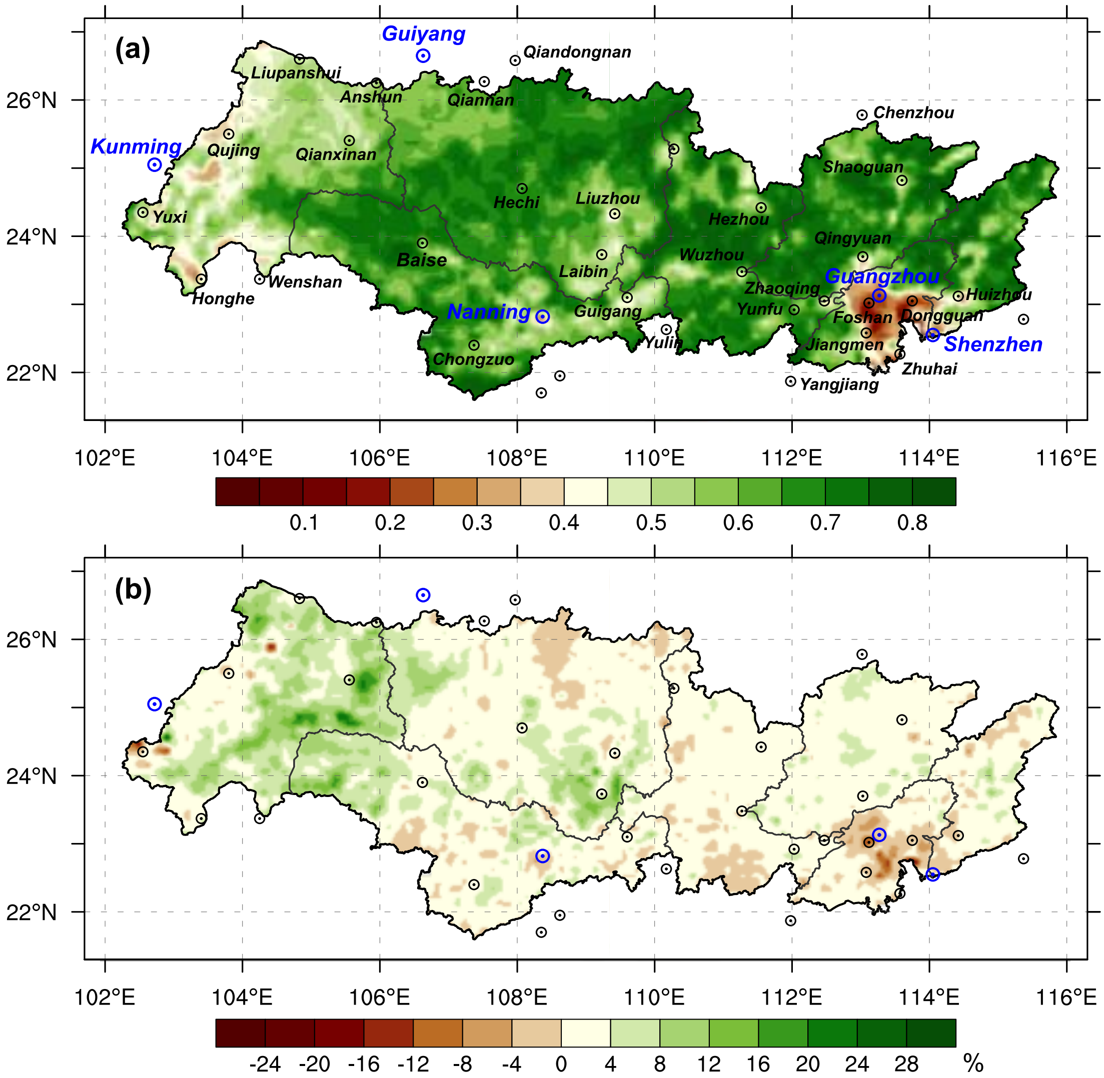

Fig. 10. The mean (a) and variation (b) of the composite exposure indicator over 1982–2017.

4.4 Ensemble mean of the NDVI- and GPP-indicated ecosystem vulnerability to drought stress

Under multiple drought scenarios, trivariate conditional probability of vegetation decline is systematically estimated following Eq. (11) to characterize ecosystem vulnerability. The occurrence of vegetation decline is typically noticed when vegetation status is lower than the 50th percentile (i.e., the long-term median). More serious vegetation loss defined by vegetation indicators below 40th, 30th and 20th percentiles is investigated as well. As the external forcing, drought stress discussed is the concurrent duration and severity separately at 5-, 10-, 20- and 30-year return levels, which is identical to the drought scenarios investigated in subsection 4.1 to ensure consistency. Sixteen combinations of the casual drought stress and the consequent vegetation decline are exhaustively analyzed, of which the results are provided in Figs. 11–12. A large likelihood of vegetation loss suggests a high degree of vulnerability.

In Figs. 11–12, a symbol *mean* at the upper-right corner of an individual panel indicates the basin mean of trivariate vegetation decline probability across the PRB. As seen in each column of the figure, the basin-average likelihood of vegetation suffering from the same decline merely diverges by 1–4% under different drought scenarios. Whereas, spatial heterogeneity is highly visible at a fine 0.1-degree resolution. In contrast to chartreuse pixels, orange and red ones denote above-50% likelihood, implying that an outcome of interest has more chance of happening in the statistical sense. In the first panel of Fig. 11, >50% possibility of vegetation decrease below 50th percentile occupies more than 58% of the PRB, and develops a northwest-southeast tilt across the Hongliu River basin and all four sub-basins of the eastern PRB. Acceleration of increase in loss probability as indicated by the emergence of more red pixels occurs in response to more stressful water shortage like 10-, 20- and 30-year droughts. It is the same case when more profound vegetation decrease (like 40th, 30th and 20th percentiles) is under investigation. In Fig. 12, the NDVI is substituted with the GPP for vegetation status characterization. A duplicate spatial pattern of high loss possibility — a northwest-southeast tilt — is disclosed as well, confirming the reliability of the probabilistic assessment outcome.

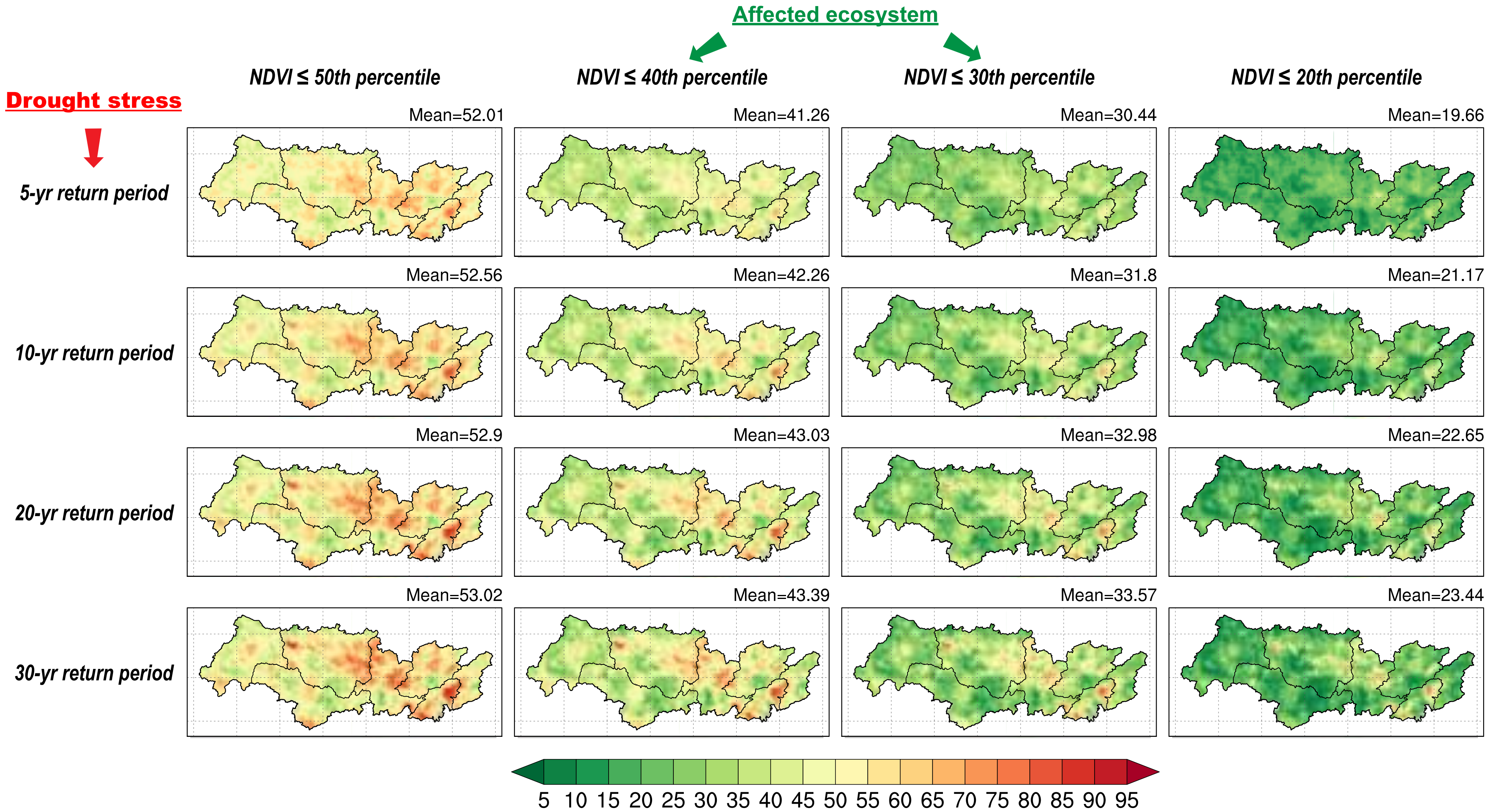

Fig. 11. The NDVI-derived vegetation decline probability conditioned on diverse drought stress.

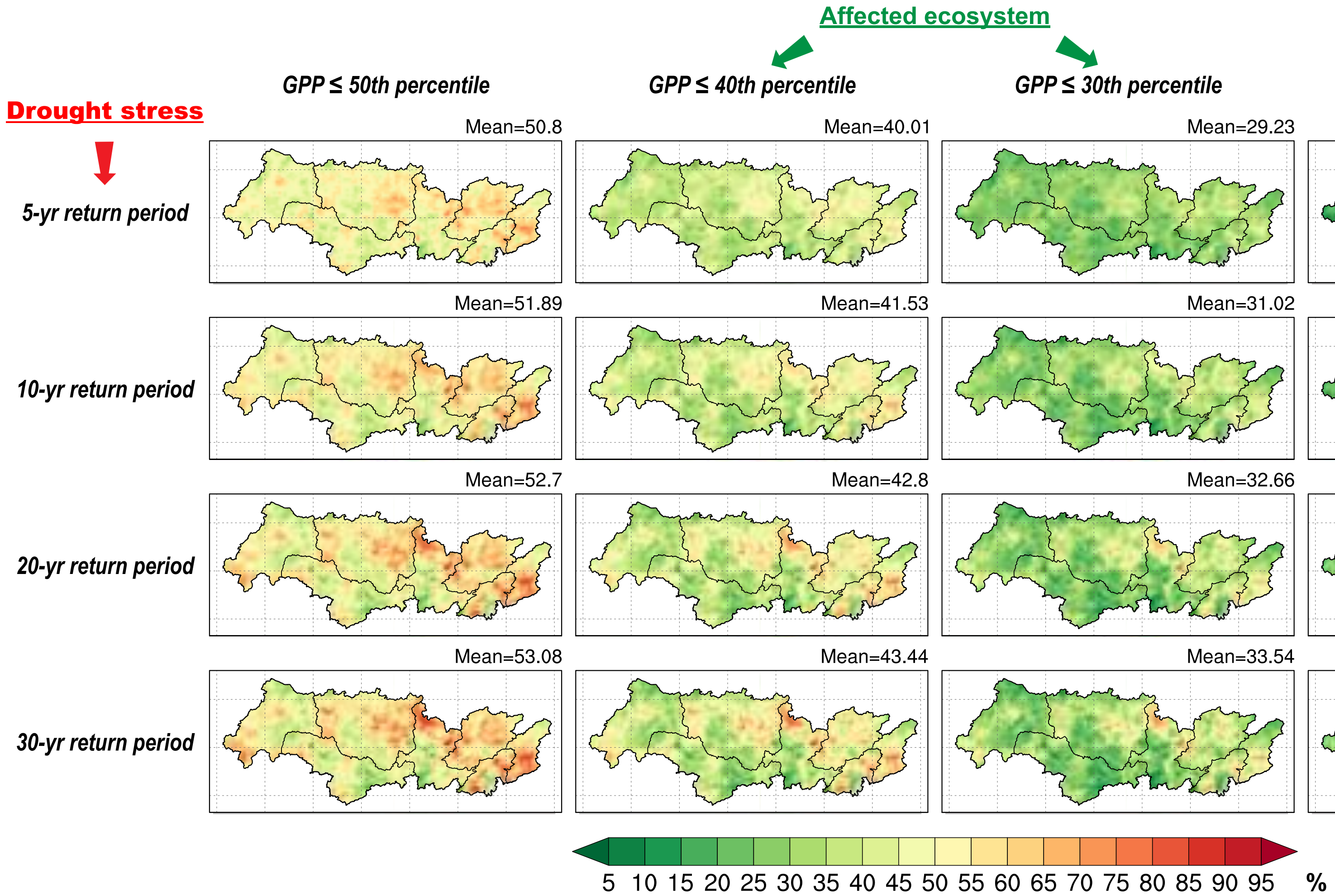

Fig. 12. The GPP-derived vegetation decline probability conditioned on diverse drought stress.

Furthermore, the NDVI- and GPP-indicated likelihood of vegetation loss (i.e., the below-50th percentile) is normalized using Eqs. (15) and (16) to derive the ensemble mean of ecosystem vulnerability. Vulnerability, by definition, is the propensity or predisposition to be adversely affected. Given deteriorating drought conditions, an increased propensity for vegetation to decline suggests exacerbating vulnerability. Under a 5-year drought scenario (Fig. 13(a)), ecosystem vulnerability varies from 0.15 to 0.74. Sub-basins in the eastern PRB, including the downstream of the West River, the North River, the East River basins and the Pearl River Delta, witness higher degree of vulnerability, which is separately 3.59%, 11.90%, 6.89% and 9.27% larger than the basin average (0.41). Vegetation in the west is less vulnerable to drought stress, especially the Nanbeipan River and the Yu River basins, of which vulnerability decreases by 9.00% and 7.28%. At 0.1-degree spatial resolution, vulnerable ecosystems (>0.5) connect the eastern Hongliu River basin, the northmost of the downstream of the West River, a large proportion of the North River basin and the eastern and southern margins of the Pearl River Delta to show northwest-southeast-directed extension, which becomes increasingly visible under more severe drought conditions at 10-, 20- and 30-year return levels (Fig. 13(b)–(d)). The abovementioned pixels with comparably high vulnerability mostly reside in agroecosystems which are highlighted in yellow in Fig. 1(d). Previous studies (Hochmuth et al., 2015; Howes et al., 2015; Taghvaeian et al., 2018; Teixeira, 2010) conducted in different climate contexts reported that plants cultivated for grain, fruit and vegetable production consume more water than natural vegetation by factors of 2 and 3. Consequently, enlarged vulnerability is more likely to emerge among water-demanding agroecosystems (especially, the rainfed) when suffering from precipitation deficits. An exceptional case is that the eastern Yu River basin where the cropland shows the greatest ground coverage across the PRB (Fig. 1(d);

Wang et al., 2021), has an unexpectedly low level of ecosystem vulnerability. According to statistics from local authorities, more than 50% of cultivated land in Nanning (243k hectares/480k hectares) and Guigang (184k hectares/320k hectares) within the domain of the eastern Yu River basin has access to irrigation facilities to cope with drought, while only 19% cropland of the eastern Hongliu River basin (140k hectares/755k hectares) has access to irrigation systems. It is reasonable to infer that appropriate human interventions, such as irrigation, can serve to regulate ecosystem vulnerability.

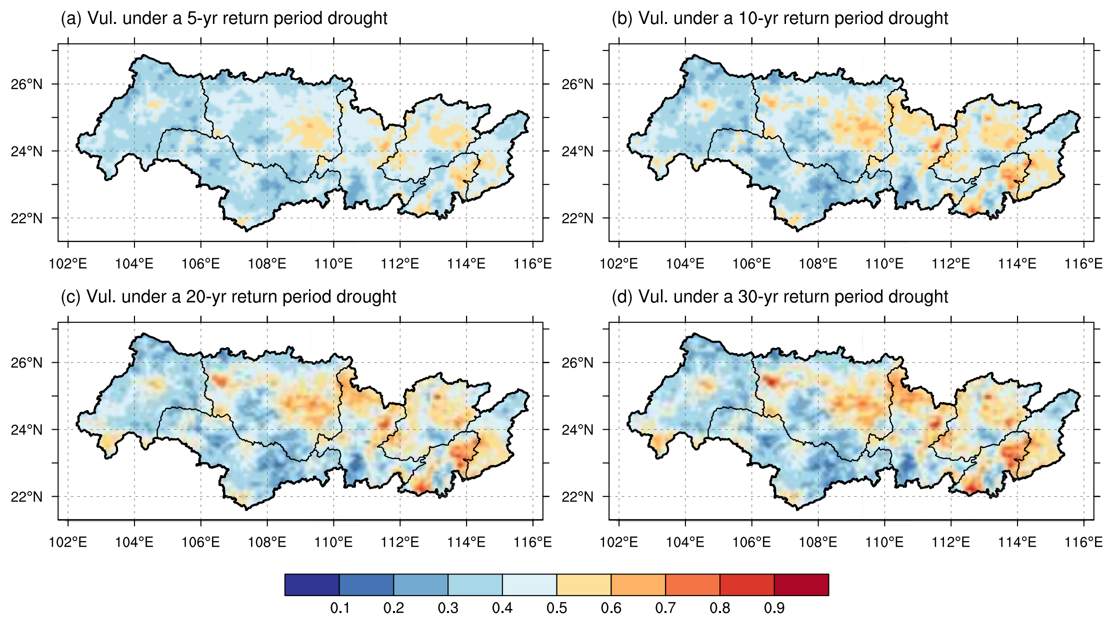

Fig. 13. Ensemble of drought-induced vegetation vulnerability derived from diverse vegetation indicators.

4.5 Time-varying ecosystem risk induced by droughts in the PRB

As defined, time-varying ecosystem risk arising from droughts is calculated as the multiplication of hazard likelihood (P_{and} representing a more stressful concurrency scenario is herein considered), ecosystem exposure and vulnerability. Risk maps at 0.1-degree spatial resolution were generated to study the spatial pattern (Figs. 14–15) and temporal dynamics (Figs. 16–17), in support of pinpointing hotspots where high risk projected to be further aggravated should receive the overriding mitigation priority.

4.5.1 Spatial pattern and temporal change of drought-induced ecosystem risk during 1982–2017

Spatial patterns become distinguishable in Fig. 14 by mapping out the mean of drought-induced ecosystem risk during 1982–2017. When a 5-year drought occurs as the external forcing, ecosystem risk is estimated to have a mean value of 0.0226 across the PRB. For individual sub-basin, ecosystems in the East River (0.0304) and the Hongliu River (0.0301) basins are uniformly at 33% higher risk compared with the PRB mean. Lower risk fluctuating around the basin mean is noted from west to east, mainly in the Nanbeipan River (0.0188), the Yu River (0.0212), the downstream of the West River (0.0191) and the North River (0.0194) basins. The Pearl River Delta (0.0137) is the least risky sub-basin where ecosystem risk deviates from the PRB average by -39%. Risk assessment conducted under an ensemble of 10-, 20- and 30-year drought scenarios also confirms the elevated levels of ecosystem risk in the East River and the Hongliu River basins. Furthermore, ecosystem risk under drought stress is clustered into three groups using the k-means algorithm to visualize the relatively high, medium and low levels within the PRB domain. As seen in Fig. 15, relatively low, medium and high levels of risk under a 5-yr return period drought are within the range of (0, 0.020], (0.020, 0.035] and (0.035, 0.065], respectively. High-risk pixels highlighted in dark golden yellow and red occupy 18.96% of the PRB, with concentration more specifically in the majority of the East River basin as well as the western and northern parts of the Hongliu River basins at 0.1-degree resolution. Medium risk corresponding to light yellow pixels dominates the rest Hongliu River basin and is more widely distributed over the middle of the Yu River basin and the western and northern Nanbeipan River basin, presenting a spatial coverage of up to 37.99% in the study area.

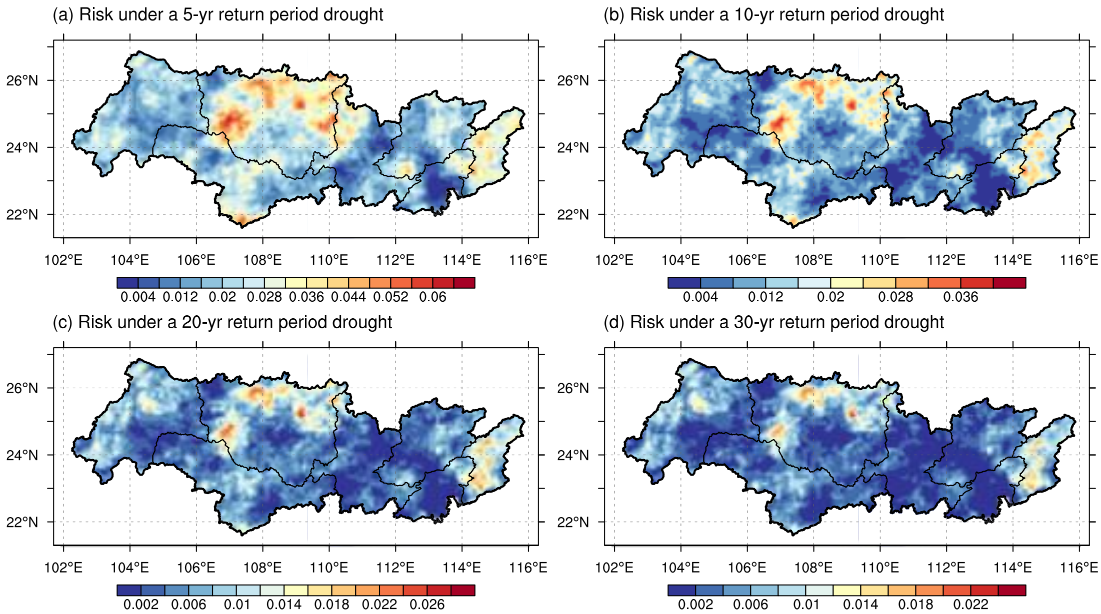

Fig. 14. Mean values of drought-related ecosystem risk in the PRB during 1982–2017.

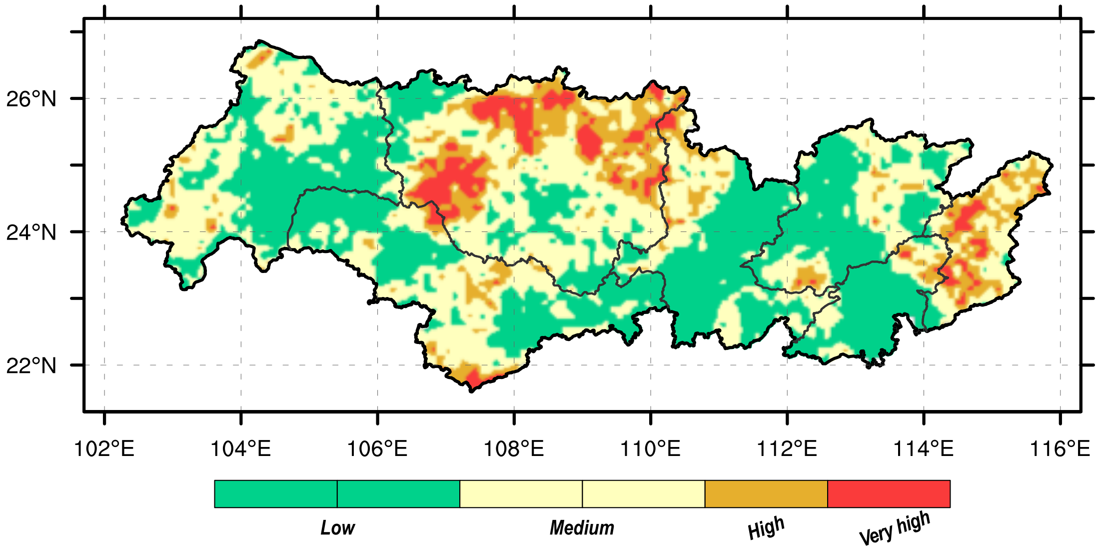

Fig. 15. Ecosystem risk clustered by the k-means method in the PRB.

In addition to spatial patterns, the proposed DERM model provides insight into how ecosystem risk varies in a changing climate. Out of a total of 4019 pixels within the scope of the PRB, 2459 (61.18%), 2548 (63.40%), 2554 (63.55%) and 2565 (63.82%) pixels witness an enlargement of risk under the stress of 5-, 10-, 20- and 30-year droughts, respectively. As depicted in Fig. 16, the increasing trend mostly occurs over the northern PRB (i.e., 74.41% of the Nanbeipan River basin, 65.08% of the downstream of the West River basin, 94.58% of the North River basin and 92.25% of the East River basin), except for the Hongliu River basin. On the contrary, more than 50% of the southern PRB accompanied by the northerly Hongliu River basin is subject to the alleviated ecosystem risk. Meanwhile, decadal analysis is performed to justify the risk alternation identified above. Fig. 17 exemplifies the decadal mean risk under the 5-year drought scenario. The PRB average risk presents an overall upward trend throughout the entire analysis period, increasing rapidly from 0.0197 in 1982–1989 to 0.0205 in 1990–1999 and 0.0274 in 2000–2009 and slightly diminishing to 0.0224 till the most recent decade (2010–2017). A westward and eastward expansion of high risk from the middle PRB (the Hongliu River basin) in 1982–1989 to the Nanbeipan River and East River basins at PRB margins in 2010–2017 finally results in the intensification of risk across most of the northern part, justifying the identified temporal alteration in ecosystem risk. Thereby, analysis of mean annual change (Fig. 16) and decadal mean (Fig. 17) of risk jointly discloses that ecosystems in more than 60% of the PRB are at amplified risk during the past four decades. Exacerbated risk prevails over the northern PRB (except for part of the Hongliu River basin) in contrast to the alleviated risk mainly in the southern part.

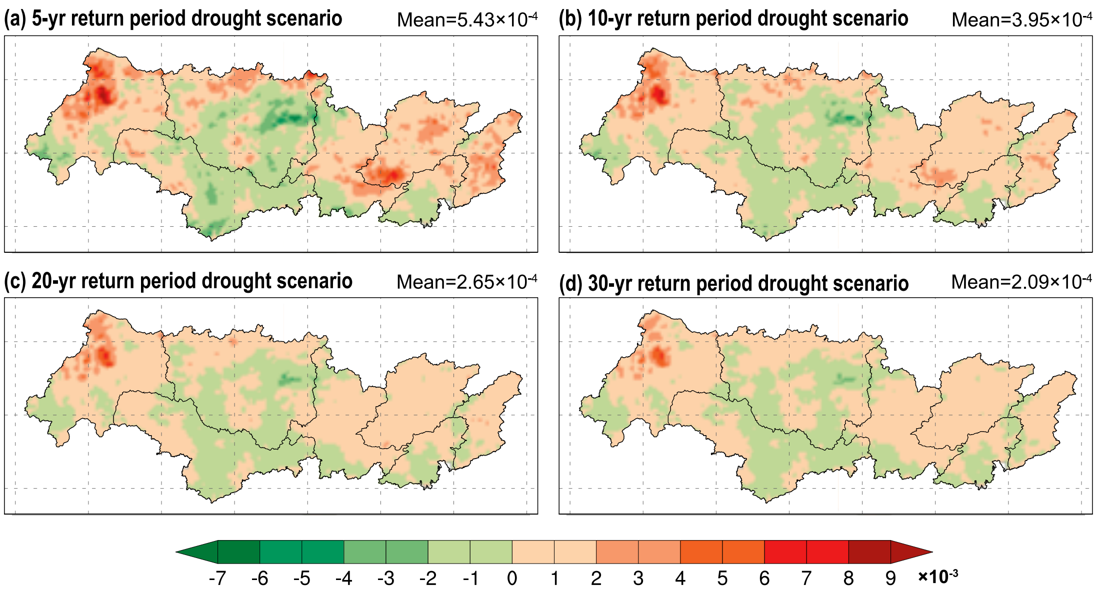

Fig. 16. Mean annual changes in drought-induced ecosystem risk during the recent four decades.

995 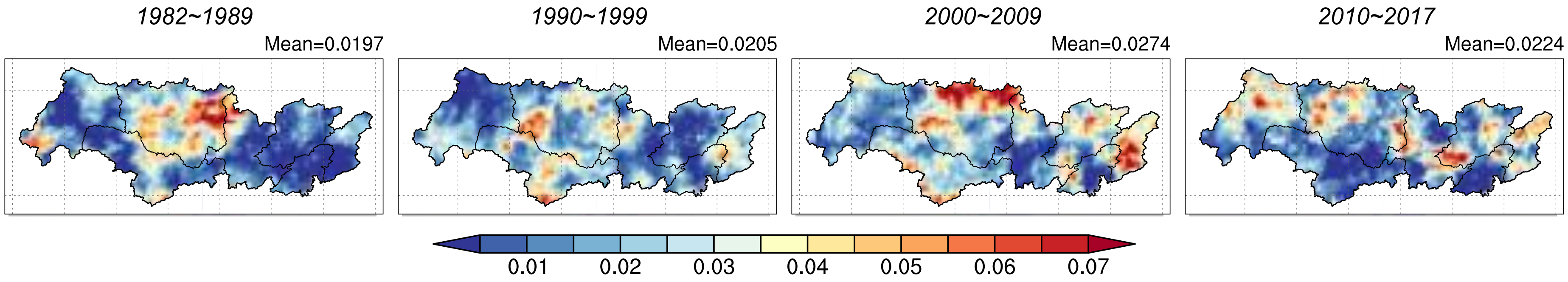

996 **Fig. 17.** Decadal mean of ecosystem risk under a 5-year drought over (a) 1982-1989, (b) 1990-1999, (c) 2000-2009 and (d) 2010-2017, respectively.

4.5.2 Hotspots of drought-induced ecosystem risk

Ultimately, the spatial pattern of risk, together with its temporal dynamic acquired from the proposed DERM model, is combined to identify risk hotspots. Additional involvement of risk change information elaborates hotspot analysis by further notifying whether there will be an acute exacerbation of ecosystem risk in the near future, which is closely associated with the performance of risk mitigation efforts in a changing climate. Pixels, where high risk is expected to continue to escalate, are the most pressing hotspots and should receive the highest priority. Out of a total of 762 high-risk pixels, 431 pixels (56.56%) showed an escalation trend (Table 4) and were therefore identified as hotspots. As depicted in Fig. 18, the most pressing hotspots of drought-induced ecosystem risk are mostly confined in the northern and western margins of the Hongliu River basin (185 pixels) and the East River basin (116 pixels). As illustrated in Figs. 9, 10 and 13, relatively high levels of bivariate drought probability and ecosystem exposure are responsible for high risk in the northern and western margins of the Hongliu River basin, while they are bivariate drought probability, exposure and vulnerability uniformly at high levels in the East River basin. As for the increasing trend in ecosystem risk, it is primarily attributed to the escalating drought probability as revealed in subsection 4.2. In addition, there is considerable potential for moderate risk to swell to high levels when an uptrend is superimposed. Related pixels can be considered as potential hotspots where early preparations are also needed to deal with the impending adverse effects. Potential hotspots highlighted in orange develop continuously in the northwestern (corresponding to 252 pixels in the Nanbeipan River basin) and northeastern (covering 263 pixels in the North River and East River basins) PRB, with some smaller patches embedded in the middle portion. Thereby, the knowledge gained in terms of spatial patterns and temporal variations facilitates an elaborate hotspot analysis by differentiating a collection of risk hotspots. In the PRB, the most pressing hotspots with the highest mitigation priority are predominantly found in the middle and eastern margins. An early preparedness plan should be made as well, to address the possible future impact upon potential hotspots that outline two space continuums across the northwestern and northeastern PRB, respectively.

Table 4 Number of pixels with above-medium risk superposed by trend information over 1982–2017

Sub-basins	High risk		Medium risk	
	Uptrend	Downtrend	Uptrend	Downtrend
The Nanbeipan River basin	25	15	**252**	86
The HongLiu basin	**185**	209	179	240
The Yu River basin	20	69	83	190
The downstream of the West River	32	31	95	59
The North River basin	34	0	**162**	16
The East River basin	**116**	7	**101**	12
The Pearl River Delta	19	0	33	19
The Whole PRB	431	331	905	622

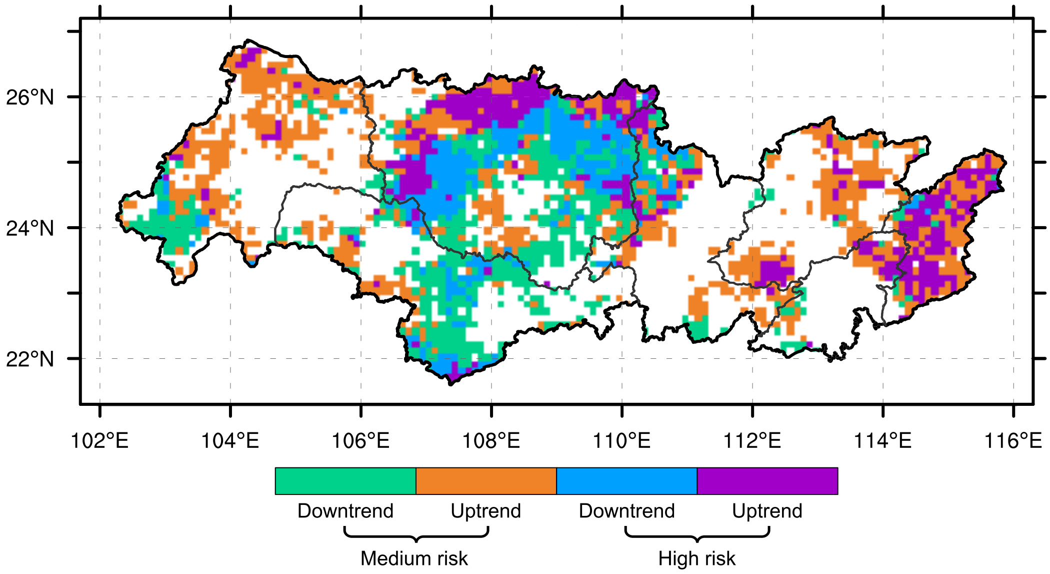

Fig. 18. High and medium risk superposed by trend information over the past four decades.

5 Discussion

Risk components are all classified into low, medium and high levels via the k-means method to facilitate attribution analysis. Risk components with dominant control over above-medium risk are finally screened out to elucidate the driving mechanism of risk and develop appropriate mitigation strategies.

It is observed in Fig. 19 that medium and high levels of drought frequency, exposure and vulnerability emerge at 90.26%, 94.06% and 74.40% of 2289 pixels having above-medium risk, respectively. Accordingly, drought frequency and exposure are found to exert more widespread influence upon the formation of above-medium risk relative to the vulnerability component. The above-medium risk may be the result of a single risk component or several ones jointly reaching medium and high levels. Fig. 19 indicates that when a single risk component is sequentially investigated, only drought frequency imposes exclusive control on above-medium risk at 45 pixels that are highlighted in red. The dominant role of drought frequency is profound in the western margin of the Nanbeipan River basin, which coincides well with where drought recurrence is at a high rate (Figs. 8–9). Drought frequency, in essence, represents the external forcing of climate extremes for risk formation. At 45 pixels identified above, risk mitigation in a way of modulating climate extremes calls for long-term collaborative efforts to alleviate climate impact upon ecosystems across the globe and thereby may not be attained in short time frames. In the remaining part covering 2240 pixels, above-medium risk is the composite result of at least two risk components reaching medium and high values. Detailly, all three risk components exceeding the medium levels are noted to take shared responsibility for above-medium risk at up to 1393 orange pixels, which is successively followed by the frequency and exposure combination (i.e., highlighted in seagreen) and the exposure and vulnerability combination (i.e., highlighted in yellow) separately acting as dominant risk drivers at 537 and 219 pixels.

In the context of global warming and the high uncertainty of future regional climate extremes (Sillmann et al., 2021), transnational climate governance over decades or even centuries is required to regulate existing drought frequencies (Lawrence et al., 2020;

Malhi et al., 2020). Buffering risk components — namely exposure and vulnerability — through broad ecosystem management activities is considered a viable way to mitigate ecosystem risks in the short term (UNISDR, 2015). For instance, lower exposure of agroecosystems to water stress can be achievable through interventions including the planting date adjustment (Kosoe & Ahmed, 2022; Lu et al., 2017) and the relocation of water-demanding crops cultivated during drought-intensive months (Ray et al., 2018).

More options can be adopted to reduce vulnerability, which allows ecosystems to co-exist with climate extremes. (Wamsler et al., 2016). For agroecosystems, supplemental irrigation (Byrareddy et al., 2021; Diatta et al., 2021) is in widespread application, which diverts alternative sources of water (mainly groundwater and impounded water in reservoirs) in order to make vegetation communities less vulnerable to insufficient atmospheric water supply. As discussed in subsection 4.4, the significant role of irrigation practices in the US (Oikonomou et al., 2019), South Africa (Araujo et al., 2016) and Europe (Orth et al., 2020) is also found in the eastern Yu River basin of the PRB. The other cluster of mitigation options manages to reduce crop lifetime water consumption through the improved water use efficiency (WUE). To achieve the goal, a cascade of molecular, biochemical and physiological modifications at a cell level can be implemented with the aid of the emerging biotechnological approaches (Hussain et al., 2018), comprising genetic makeup manipulation for breeding drought-tolerant crop species, and the exogenous application of compatible solutes (soluble sugars, for instance; Dien et al., 2019) for lowering osmotic potential and thereby maintaining tissue water content, hormonal or non-hormonal plant growth regulators (abscisic acid and jasmonates; Fugate et al., 2018; Mega et al., 2019) for triggering plant defense response (for instance, water-saving antitranspirant response) and mineral nutrients (phosphorus and potassium additions; Ahmad et al., 2018; Nawaz et al., 2020) for drought stress alleviations. Besides, several management practices, although relatively limited, can be designed to diminish vulnerability of natural ecosystems like forests and grassland covering up to 61.92% and 11.84% of the PRB (Fig. 1). Forest ecosystems of the PRB account for the highest proportion (greater than 47% in 2021) of national wood production, whilst being frequently perturbed by water scarcity. Density reduction through silvicultural thinning treatments might be advocated as a near-term solution to mitigate forest vulnerability to drought stress (Navarro-Cerrillo et al., 2019; Restaino et al., 2019; Zhang et al., 2021) because of such efforts in favor of increased water availability to the remaining trees during drought episodes (D'Amato et al., 2013). With regard to grassland ecosystems, vulnerability, to a large extent, originates from the fact that persistent water shortage reduces mobility and availability of nutrients indispensable for plant functioning and metabolism (Araya et al., 2022; Meisser et al., 2019). To enhance resistance to droughts, biodiversity restoration management (De Boeck et al., 2018; Isbell et al., 2015) can be conducted as a way of enhancing nutrient uptake and WUE by adding key functional groups of plants and microorganisms to grassland communities. Previous studies have revealed that some candidate functional biomes are legume species with N-fixing rhizobia associations (Cole et al., 2019) and biotechnologically developed phosphorus-solubilizing microbes (Kour et al., 2019), the presence of which has potential to confer higher resistance (i.e., lower vulnerability) of the sub-alpine meadows also predominantly distributed at the western margin of the current study area (Fig. 1). Overall, the human practices described above illustrate a variety of efforts to buffer vulnerability by following pathways that increase water availability to individual plants or reduce water demand through the improved water use efficiency. Under ideal conditions, 2,240 pixels, representing 55.83% of the total PRB, are expected to have moderate or higher ecosystem risk mitigated if appropriate measures are taken to mitigate ecosystem exposure and vulnerability.

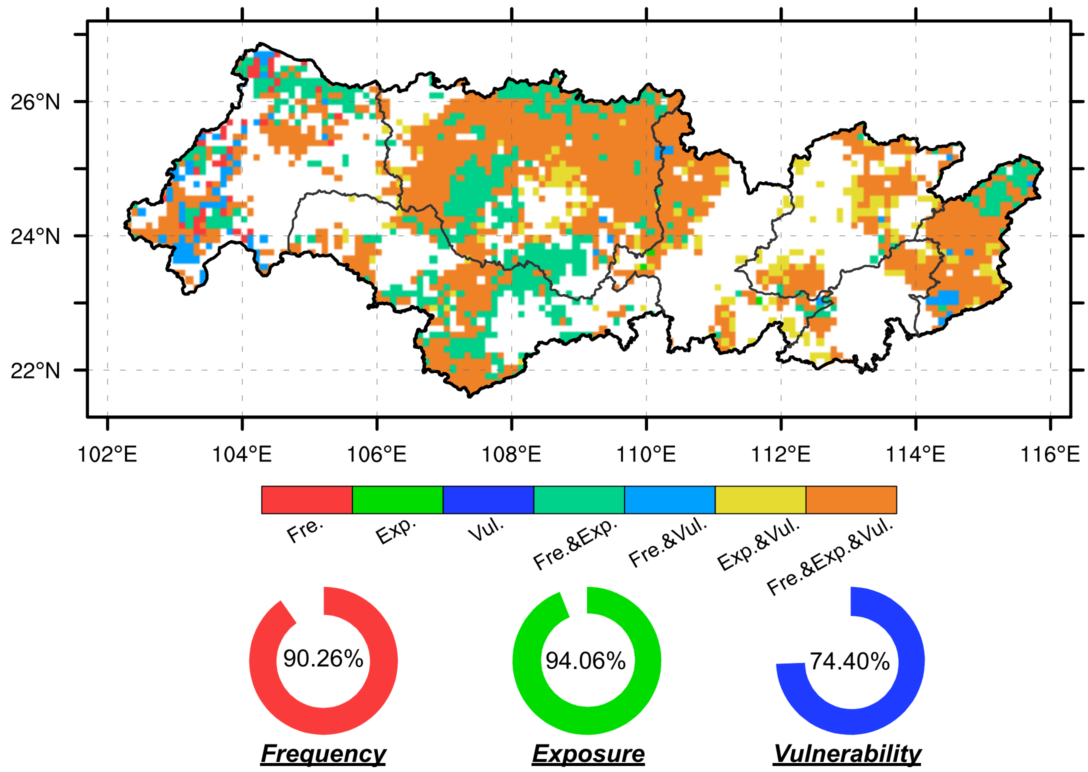

Fig. 19. Ecosystem risk is high and medium when the three risk factors are at a medium or higher level.

6 Conclusions

Ecosystems, which cover 28.26% of the Earth's surface, are extensively at risk worldwide when suffering from droughts — a major abiotic stressor receiving increased attention in a warming climate. Drought-induced ecosystem risk can propagate rapidly into the connected human communities via the mismatch between ecosystem service supply and human demand, thereby reinforcing the necessity to specifically evaluate ecosystem risk imposed by droughts and climate extremes. In addition, dynamic risks may arise from time-variant risk determinants — hazard frequency, exposure and vulnerability — within anthropogenically-forced nonstationary environments. The expanded knowledge of how and to what extent risk evolves is indispensable for updating risk-based proactive mitigation strategies with desirable performance in the upcoming decades. To this end, the present study develops a DERM model to investigate the composition, spatio-temporal variability as well as driving mechanism of time-varying ecosystem risk under the stress of climate extremes. In the DERM model, bivariate drought exceedance probability as the hazard component of risk is initially calculated jointly considering univariate and bivariate nonstationarity of duration and severity, with the aid of the GAMLSS model and dynamic copula. Meanwhile, a two-dimensional indicator coupling vegetation coverage and biomass quantity is formulated to characterize ecosystem exposure through a non-compensatory approach. Trivariate likelihood of vegetation loss (quantified using the NDVI and GPP decline) given arbitrary multivariate drought condition (i.e., the pairwise duration and severity) is derived as an intuitive metric for ecosystem vulnerability to drought stress. Ultimately, dynamic risk is calculated by multiplying time-variant drought frequency, ecosystem exposure and vulnerability, followed by a chain of post analysis including the identification of spatio-temporal variability, the most pressing risk hotspots and the main drivers of above-medium risk for proactive mitigation planning.

Time-varying ecosystem risk at 0.1-degree resolution was assessed during 1982–2017 in the PRB, China, where recurrent precipitation deficiency exerts a significant control on ecosystem functioning and productivity. Results indicate that meteorological droughts revisit the middle PRB at higher frequencies, which have characteristics of shorter duration and lower severity. In contrast, droughts in the eastern and western margins, although less frequent, become prolonged and severe. Mean ecosystem exposure to drought stress fluctuates within a small range from 0.48 to 0.66 across seven sub-basins and exhibits less pronounced heterogeneity over space. Intensification of exposure over the 86.12% PRB is more pronounced in the karst western proportion as a result of vegetation restoration, whilst a drastic decline with the maximum of -25.41% over the Pearl River Delta is due to rapid urban expansion over the past decades. As the third risk component, ecosystem vulnerability at relatively high levels (>0.5) mostly resides in the eastern PRB and shows northwest-southeast-directed extension. Greater vulnerability is found amongst water-demanding agroecosystems, which can be beneficially modulated by irrigation practices. Ultimately, dynamic risk analysis incorporating the foregoing risk determinants discloses that high and medium risk occupies 18.96% and 37.99% of the PRB, respectively. More than 60% of the PRB (i.e., the northern PRB except for part of the Hongliu River basin) is at amplified risk in contrast to the alleviated risk mainly in the southern part. Furthermore, the most pressing hotspots where high risk superimposed by an escalating trend takes the overriding mitigation priority are predominantly at the northern and western margins of the Hongliu River basin (185 pixels) and the East River basin (116 pixels). Drought frequency and exposure are found to exert more widespread influence upon the formation of above-medium risk relative to the vulnerability component in the PRB.

Overall, the proposed DERM model can be used for the quantification of drought impacts on ecosystems and has the potential to be applied in other regions for the mitigation of drought-induced ecosystem risk in a changing climate. The developed model also allows more flexibility in the substitution of droughts with floods, heatwaves, chilling, wildfires, compound extreme events (Phillips et al., 2020), insect pests (Rasche & Taylor, 2019) and infectious diseases (Hassell et al., 2021) as a way to identify highly risky ecosystems under diverse abiotic and biotic stress and understand how risk evolves under future climate scenarios. Additionally, terrestrial ecosystems are tightly coupled to human communities in the functional domain including ecosystem service provision and the secondary effect of ecosystem disruption across a broader spatial scale. Ecosystem risk may thereby spread out and exacerbate drought-induced risk to human settlements due to the loss of vital services highly valued by human beings, which is termed as cascading risk (Pescaroli & Alexander, 2018). Therefore, the modeling of causal interactions between natural and anthropogenic systems, the subsequent identification of cascading risk pathways (Suk et al., 2020) and the initiation of appropriate measures to minimize risk propagation rate might be some significant topics deserving further investigation.

Acknowledgments

This study was jointly funded by the National Natural Science Foundation of China (grant number 52009100 and U2243216), China Postdoctoral Science Foundation (grant number 2021M692602), Yinshanbeilu Grassland Eco-hydrology National Observation and Research Station, China Institute of Water Resources and Hydropower Research (grant number YSS2022006) and the Doctorate Innovation Funding of Xi'an University of Technology (grant number 310-252072112).

Data availability

Precipitation records were freely acquired from the National Tibetan Plateau/Third Pole Environment Data Center (http://data.tpdc.ac.cn/en/data/8028b944-daaa-4511-8769-965612652c49/). The NDVI was provided by the NOAA's Climate Data Records (https://www.ncei.noaa.gov/data/avhrr-land-normalized-difference-vegetation-index/access/). The utilized FVC, LAI and GPP were collected from the Global Land Surface Satellite (GLASS) product suite (version 4) accessible via http://www.glass.umd.edu/.

References

Aerts, J. C. J. H., Botzen, W. J., Clarke, K. C., Cutter, S. L., Hall, J. W., Merz, B., et al. (2018). Integrating human behaviour dynamics into flood disaster risk assessment. *Nature Climate Change*, *8*(3), 193-199. https://doi.org/10.1038/s41558-018-0085-1

Ahmad, Z., Anjum, S., Waraich, E. A., Ayub, M. A., Ahmad, T., Tariq, R. M. S., et al. (2018). Growth, physiology, and biochemical activities of plant responses with foliar potassium application under drought stress – a review. *Journal of Plant Nutrition*, *41*(13), 1734-1743. https://doi.org/10.1080/01904167.2018.1459688

Ahmadalipour, A., Moradkhani, H., Castelletti, A., & Magliocca, N. (2019). Future drought risk in Africa: Integrating vulnerability, climate change, and population growth. *Science of The Total Environment*, *662*, 672-686. https://doi.org/10.1016/j.scitotenv.2019.01.278

Amirataee, B., Montaseri, M., & Rezaie, H. (2020). An advanced data collection procedure in bivariate drought frequency analysis. *Hydrological Processes*, *34*(21), 4067-4082. https://doi.org/10.1002/hyp.13866

Angeon, V., & Bates, S. (2015). Reviewing Composite Vulnerability and Resilience

Indexes: A Sustainable Approach and Application. *World Development*, *72*, 140-162. https://doi.org/10.1016/j.worlddev.2015.02.011

Araujo, J. A., Abiodun, B. J., & Crespo, O. (2016). Impacts of drought on grape yields in Western Cape, South Africa. *Theoretical and Applied Climatology*, *123*(1), 117-130. https://doi.org/10.1007/s00704-014-1336-3

Araya, A., Jha, P. K., Zambreski, Z., Faye, A., Ciampitti, I. A., Min, D., et al. (2022). Evaluating crop management options for sorghum, pearl millet and peanut to minimize risk under the projected midcentury climate scenario for different locations in Senegal. *Climate Risk Management*, 36, 100436. https://doi.org/10.1016/j.crm.2022.100436

Bachmair, S., Svensson, C., Prosdocimi, I., Hannaford, J., & Stahl, K. (2017). Developing drought impact functions for drought risk management. *Nat. Hazards Earth Syst. Sci.*, *17*(11), 1947-1960. https://doi.org/10.5194/nhess-17-1947-2017

Balogun, V. S., & Onokerhoraye, A. G. (2022). Climate change vulnerability mapping across ecological zones in Delta State, Niger Delta Region of Nigeria. *Climate Services*, 27, 100304. https://doi.org/10.1016/j.cliser.2022.100304

Blauhut, V., Stahl, K., Stagge, J. H., Tallaksen, L. M., De Stefano, L., & Vogt, J. (2016). Estimating drought risk across Europe from reported drought impacts, drought indices, and vulnerability factors. *Hydrol. Earth Syst. Sci.*, *20*(7), 2779-2800. https://doi.org/10.5194/hess-20-2779-2016

Brèteau-Amores, S., Brunette, M., & Davi, H. (2019). An Economic Comparison of Adaptation Strategies Towards a Drought-induced Risk of Forest Decline. *Ecological Economics*, *164*, 106294. https://doi.org/10.1016/j.ecolecon.2019.04.006

Bucchia, B., & Wendler, M. (2017). Change-point detection and bootstrap for Hilbert space valued random fields. *Journal of Multivariate Analysis*, *155*, 344-368. https://doi.org/10.1016/j.jmva.2017.01.007

Byers, E., Gidden, M., Leclère, D., Balkovic, J., Burek, P., Ebi, K., et al. (2018). Global exposure and vulnerability to multi-sector development and climate change hotspots. *Environmental Research Letters*, *13*(5), 055012. https://doi.org/10.1088/1748-9326/aabf45

Byrareddy, V., Kouadio, L., Mushtaq, S., Kath, J., & Stone, R. (2021). Coping with drought: Lessons learned from robusta coffee growers in Vietnam. *Climate*

Services, 22, 100229. https://doi.org/10.1016/j.cliser.2021.100229

Campbell, J. E., Berry, J. A., Seibt, U., Smith, S. J., Montzka, S. A., Launois, T., et al. (2017). Large historical growth in global terrestrial gross primary production. *Nature*, *544*(7648), 84-87. https://doi.org/10.1038/nature22030

Carrão, H., Naumann, G., & Barbosa, P. (2016). Mapping global patterns of drought risk: An empirical framework based on sub-national estimates of hazard, exposure and vulnerability. *Global Environmental Change*, *39*, 108-124. https://doi.org/10.1016/j.gloenvcha.2016.04.012

Chakraborty, A., & Joshi, P. K. (2016). Mapping disaster vulnerability in India using analytical hierarchy process. *Geomatics, Natural Hazards and Risk*, *7*(1), 308-325. https://doi.org/10.1080/19475705.2014.897656

Chebana, F., Ouarda, T. B. M. J., & Duong, T. C. (2013). Testing for multivariate trends in hydrologic frequency analysis. *Journal of Hydrology*, *486*, 519-530. https://doi.org/10.1016/j.jhydrol.2013.01.007

Chen, C., Park, T., Wang, X., Piao, S., Xu, B., Chaturvedi, R. K., et al. (2019). China and India lead in greening of the world through land-use management. *Nature Sustainability*, *2*(2), 122-129. https://doi.org/10.1038/s41893-019-0220-7

Cochavi, A., Amer, M., Stern, R., Tatarinov, F., Migliavacca, M., & Yakir, D. (2021). Differential responses to two heatwave intensities in a Mediterranean citrus orchard are identified by combining measurements of fluorescence and carbonyl sulfide (COS) and CO2 uptake. *New Phytologist*, *230*(4), 1394-1406. https://doi.org/10.1111/nph.17247

Cole, A. J., Griffiths, R. I., Ward, S. E., Whitaker, J., Ostle, N. J., & Bardgett, R. D. (2019). Grassland biodiversity restoration increases resistance of carbon fluxes to drought. *Journal of Applied Ecology*, *56*(7), 1806-1816. https://doi.org/10.1111/1365-2664.13402

D'Amato, A. W., Bradford, J. B., Fraver, S., & Palik, B. J. (2013). Effects of thinning on drought vulnerability and climate response in north temperate forest ecosystems. *Ecological Applications*, *23*(8), 1735-1742. https://doi.org/10.1890/13-0677.1

Dai, M., Huang, S., Huang, Q., Leng, G., Guo, Y., Wang, L., et al. (2020). Assessing agricultural drought risk and its dynamic evolution characteristics. *Agricultural Water Management*, *231*, 106003. https://doi.org/10.1016/j.agwat.2020.106003

Dalezios, N. R., Blanta, A., Spyropoulos, N. V., & Tarquis, A. M. (2014). Risk identification of agricultural drought for sustainable Agroecosystems. *Nat. Hazards Earth Syst. Sci.*, *14*(9), 2435-2448. https://doi.org/10.5194/nhess-14-2435-2014

Das, J., Jha, S., & Goyal, M. K. (2020). Non-stationary and copula-based approach to assess the drought characteristics encompassing climate indices over the Himalayan states in India. *Journal of Hydrology*, *580*, 124356. https://doi.org/https://doi.org/10.1016/j.jhydrol.2019.124356

De Boeck, H. J., Bloor, J. M. G., Kreyling, J., Ransijn, J. C. G., Nijs, I., Jentsch, A., & Zeiter, M. (2018). Patterns and drivers of biodiversity–stability relationships under climate extremes. *Journal of Ecology*, *106*(3), 890-902. https://doi.org/10.1111/1365-2745.12897

Diatta, A. A., Min, D., & Jagadish, S. V. K. (2021). Chapter Two - Drought stress responses in non-transgenic and transgenic alfalfa—Current status and future research directions. In D. L. Sparks (Ed.), *Advances in Agronomy* (Vol. 170, pp. 35-100). Academic Press. https://doi.org/10.1016/bs.agron.2021.06.002

Dien, D. C., Mochizuki, T., & Yamakawa, T. (2019). Effect of various drought stresses and subsequent recovery on proline, total soluble sugar and starch metabolisms in Rice (Oryza sativa L.) varieties. *Plant Production Science*, *22*(4), 530-545. https://doi.org/10.1080/1343943X.2019.1647787

Diffenbaugh, N. S., Singh, D., Mankin, J. S., Horton, D. E., Swain, D. L., Touma, D., et al. (2017). Quantifying the influence of global warming on unprecedented extreme climate events. *Proceedings of the National Academy of Sciences*, *114*(19), 4881-4886. https://doi.org/10.1073/pnas.1618082114

Dong, T., Liu, J., Qian, B., He, L., Liu, J., Wang, R., et al. (2020). Estimating crop biomass using leaf area index derived from Landsat 8 and Sentinel-2 data. *ISPRS Journal of Photogrammetry and Remote Sensing*, *168*, 236-250. https://doi.org/10.1016/j.isprsjprs.2020.08.003

Du, J., Fu, Q., Fang, S., Wu, J., He, P., & Quan, Z. (2019). Effects of rapid urbanization on vegetation cover in the metropolises of China over the last four decades. *Ecological Indicators*, *107*, 105458. https://doi.org/10.1016/j.ecolind.2019.105458

Du, J., Quan, Z., Fang, S., Liu, C., Wu, J., & Fu, Q. (2020). Spatiotemporal changes in vegetation coverage and its causes in China since the Chinese economic reform. *Environmental Science and Pollution Research*, *27*(1), 1144-1159.

https://doi.org/10.1007/s11356-019-06609-6

Fang, W., Huang, S., Huang, G., Huang, Q., Wang, H., Wang, L., et al. (2019a). Copulas-based risk analysis for inter-seasonal combinations of wet and dry conditions under a changing climate. *International Journal of Climatology*, 39(4), 2005-2021. https://doi.org/https://doi.org/10.1002/joc.5929

Fang, W., Huang, S., Huang, Q., Huang, G., Wang, H., Leng, G., et al. (2019b). Probabilistic assessment of remote sensing-based terrestrial vegetation vulnerability to drought stress of the Loess Plateau in China. *Remote Sensing of Environment*, *232*, 111290. https://doi.org/10.1016/j.rse.2019.111290

Fang, W., Huang, S., Huang, Q., Huang, G., Wang, H., Leng, G., et al. (2019c). Bivariate probabilistic quantification of drought impacts on terrestrial vegetation dynamics in mainland China. *Journal of Hydrology*, *577*, 123980. https://doi.org/10.1016/j.jhydrol.2019.123980

Fatichi, S., & Pappas, C. (2017). Constrained variability of modeled T:ET ratio across biomes. *Geophysical Research Letters*, *44*(13), 6795-6803. https://doi.org/10.1002/2017GL074041

Favre, A.-C., El Adlouni, S., Perreault, L., Thiémonge, N., & Bobée, B. (2004). Multivariate hydrological frequency analysis using copulas. *Water Resources Research*, *40*(1), W01101. https://doi.org/10.1029/2003WR002456

Feng, S., & Fu, Y. F. (2009). Seasonal Characteristics of Precipitation Occurrences in the Core Area of the Subtropical High. *Acta Meteorologica Sinica*, *23*(6), 681-690.

Field, C. B., Barros, V., Stocker, T. F., & Dahe, Q. (2012). *Managing the risks of extreme events and disasters to advance climate change adaptation: special report of the intergovernmental panel on climate change*. Cambridge University Press.

Fugate, K. K., Lafta, A. M., Eide, J. D., Li, G., Lulai, E. C., Olson, L. L., et al. (2018). Methyl jasmonate alleviates drought stress in young sugar beet (Beta vulgaris L.) plants. *Journal of Agronomy and Crop Science*, *204*(6), 566-576. https://doi.org/10.1111/jac.12286

Galluccio, L., Michel, O., Comon, P., & Hero, A. O. (2012). Graph based k-means clustering. *Signal Processing*, *92*(9), 1970-1984. https://doi.org/10.1016/j.sigpro.2011.12.009

Ganguli, P., & Coulibaly, P. (2017). Does nonstationarity in rainfall require nonstationary intensity–duration–frequency curves? *Hydrol. Earth Syst. Sci.*, *21*(12), 6461-6483. https://doi.org/10.5194/hess-21-6461-2017

Gombay, E., & Horváth, L. (1999). Change-points and bootstrap. *Environmetrics*, *10*(6), 725-736. https://doi.org/10.1002/(SICI)1099-095X(199911/12)10:6<725::AID-ENV387>3.0.CO;2-K

Gonzalez, P., Neilson, R. P., Lenihan, J. M., & Drapek, R. J. (2010). Global patterns in the vulnerability of ecosystems to vegetation shifts due to climate change. *Global Ecology and Biogeography*, *19*(6), 755-768. https://doi.org/10.1111/j.1466-8238.2010.00558.x

González Tánago, I., Urquijo, J., Blauhut, V., Villarroya, F., & De Stefano, L. (2016). Learning from experience: a systematic review of assessments of vulnerability to drought. *Natural Hazards*, *80*(2), 951-973. https://doi.org/10.1007/s11069-015-2006-1

Hagenlocher, M., Meza, I., Anderson, C. C., Min, A., Renaud, F. G., Walz, Y., et al. (2019). Drought vulnerability and risk assessments: state of the art, persistent gaps, and research agenda. *Environmental Research Letters*, *14*(8), 083002. https://doi.org/10.1088/1748-9326/ab225d

Han, H., Gao, H., Huang, Y., Chen, X., Chen, M., & Li, J. (2019). Effects of drought on freshwater ecosystem services in poverty-stricken mountain areas. *Global Ecology and Conservation*, *17*, e00537. https://doi.org/10.1016/j.gecco.2019.e00537

Hassell, J. M., Newbold, T., Dobson, A. P., Linton, Y.-M., Franklinos, L. H. V., Zimmerman, D., & Pagenkopp Lohan, K. M. (2021). Towards an ecosystem model of infectious disease. *Nature Ecology & Evolution*, *5*(7), 907-918. https://doi.org/10.1038/s41559-021-01454-8

Hochmuth, H., Thevs, N., & He, P. (2015). Water allocation and water consumption of irrigation agriculture and natural vegetation in the Heihe River watershed, NW China. *Environmental Earth Sciences*, *73*(9), 5269-5279. https://doi.org/10.1007/s12665-014-3773-9

Hoque, M. A.-A., Pradhan, B., Ahmed, N., & Sohel, M. S. I. (2021). Agricultural drought risk assessment of Northern New South Wales, Australia using geospatial techniques. *Science of The Total Environment*, *756*, 143600. https://doi.org/10.1016/j.scitotenv.2020.143600

Howes, D. J., Fox, P., & Hutton, P. H. (2015). Evapotranspiration from Natural Vegetation in the Central Valley of California: Monthly Grass Reference-Based

Vegetation Coefficients and the Dual Crop Coefficient Approach. *Journal of Hydrologic Engineering*, *20*(10). https://doi.org/10.1061/(asce)he.1943-5584.0001162

Hussain, H. A., Hussain, S., Khaliq, A., Ashraf, U., Anjum, S. A., Men, S., & Wang, L. (2018). Chilling and Drought Stresses in Crop Plants: Implications, Cross Talk, and Potential Management Opportunities. *Frontiers in Plant Science*, *9*, 393. https://doi.org/10.3389/fpls.2018.00393

Isbell, F., Craven, D., Connolly, J., Loreau, M., Schmid, B., Beierkuhnlein, C., et al. (2015). Biodiversity increases the resistance of ecosystem productivity to climate extremes. *Nature*, *526*(7574), 574-577. https://doi.org/10.1038/nature15374

Jahangoshai Rezaee, M., Eshkevari, M., Saberi, M., & Hussain, O. (2021). GBK-means clustering algorithm: An improvement to the K-means algorithm based on the bargaining game. *Knowledge-Based Systems*, *213*, 106672. https://doi.org/10.1016/j.knosys.2020.106672

Jayanthi, H., Husak, G. J., Funk, C., Magadzire, T., Adoum, A., & Verdin, J. P. (2014). A probabilistic approach to assess agricultural drought risk to maize in Southern Africa and millet in Western Sahel using satellite estimated rainfall. *International Journal of Disaster Risk Reduction*, *10*, 490-502. https://doi.org/10.1016/j.ijdrr.2014.04.002

Jehanzaib, M., Shah, S. A., Yoo, J., & Kim, T. W. (2020). Investigating the impacts of climate change and human activities on hydrological drought using non-stationary approaches. *Journal of Hydrology*, *588*, 125052. https://doi.org/https://doi.org/10.1016/j.jhydrol.2020.125052

Jia, H., Wang, J., Cao, C., Pan, D., & Shi, P. (2012). Maize drought disaster risk assessment of China based on EPIC model. *International Journal of Digital Earth*, *5*(6), 488-515. https://doi.org/10.1080/17538947.2011.590535

Jia, K., Yang, L., Liang, S., Xiao, Z., Zhao, X., Yao, Y., et al. (2019). Long-Term Global Land Surface Satellite (GLASS) Fractional Vegetation Cover Product Derived From MODIS and AVHRR Data. *IEEE Journal of Selected Topics in Applied Earth Observations and Remote Sensing*, *12*(2), 508-518. https://doi.org/10.1109/JSTARS.2018.2854293

Jiang, C., Xiong, L., Xu, C.-Y., & Guo, S. (2015). Bivariate frequency analysis of nonstationary low-flow series based on the time-varying copula. *Hydrological*

Processes, *29*(6), 1521-1534. https://doi.org/10.1002/hyp.10288

Keen, R. M., Voelker, S. L., Wang, S.-Y. S., Bentz, B. J., Goulden, M. L., Dangerfield, C. R., Reed, C. C., Hood, S. M., Csank, A. Z., Dawson, T. E., Merschel, A. G., & Still, C. J. (2022). Changes in tree drought sensitivity provided early warning signals to the California drought and forest mortality event. Global Change Biology, 28, 1119-1132. https://doi.org/10.1111/gcb.15973

Kelman, I. (2018). Lost for Words Amongst Disaster Risk Science Vocabulary? *International Journal of Disaster Risk Science*, *9*(3), 281-291. https://doi.org/10.1007/s13753-018-0188-3

Koks, E. E., Jongman, B., Husby, T. G., & Botzen, W. J. W. (2015). Combining hazard, exposure and social vulnerability to provide lessons for flood risk management. *Environmental Science & Policy*, *47*, 42-52. https://doi.org/10.1016/j.envsci.2014.10.013

Koks, E. E., Rozenberg, J., Zorn, C., Tariverdi, M., Vousdoukas, M., Fraser, S. A., et al. (2019). A global multi-hazard risk analysis of road and railway infrastructure assets. *Nature Communications*, *10*(1), 2677. https://doi.org/10.1038/s41467-019-10442-3

Kosoe, E. A., & Ahmed, A. (2022). Climate change adaptation strategies of cocoa farmers in the Wassa East District: Implications for climate services in Ghana. *Climate Services*, 26, 100289. https://doi.org/10.1016/j.cliser.2022.100289

Kour, D., Rana, K. L., Yadav, A. N., Yadav, N., Kumar, V., Kumar, A., et al. (2019). Drought-Tolerant Phosphorus-Solubilizing Microbes: Biodiversity and Biotechnological Applications for Alleviation of Drought Stress in Plants. In R. Z. Sayyed, N. K. Arora, & M. S. Reddy (Eds.), *Plant Growth Promoting Rhizobacteria for Sustainable Stress Management : Volume 1: Rhizobacteria in Abiotic Stress Management* (pp. 255-308). Springer Singapore. https://doi.org/10.1007/978-981-13-6536-2_13

Kumar, R., Musuuza, J. L., Van Loon, A. F., Teuling, A. J., Barthel, R., Ten Broek, J., et al. (2016). Multiscale evaluation of the Standardized Precipitation Index as a groundwater drought indicator. *Hydrol. Earth Syst. Sci.*, *20*(3), 1117-1131. https://doi.org/10.5194/hess-20-1117-2016

Kwon, H.-H., & Lall, U. (2016). A copula-based nonstationary frequency analysis for the 2012–2015 drought in California. *Water Resources Research*, *52*(7), 5662-5675. https://doi.org/10.1002/2016WR018959

Lawrence, J., Blackett, P., & Cradock-Henry, N. A. (2020). Cascading climate change impacts and implications. *Climate Risk Management*, *29*, 100234. https://doi.org/10.1016/j.crm.2020.100234

Leng, G., & Hall, J. (2019). Crop yield sensitivity of global major agricultural countries to droughts and the projected changes in the future. *Science of The Total Environment*, *654*, 811-821. https://doi.org/10.1016/j.scitotenv.2018.10.434

Li, J., Peng, S., & Li, Z. (2017). Detecting and attributing vegetation changes on China's Loess Plateau. *Agricultural and Forest Meteorology*, *247*, 260-270. https://doi.org/10.1016/j.agrformet.2017.08.005

Li, J., Wang, Z., Wu, X., Guo, S., & Chen, X. (2020). Flash droughts in the Pearl River Basin, China: Observed characteristics and future changes. *Science of The Total Environment*, *707*, 136074. https://doi.org/10.1016/j.scitotenv.2019.136074

Li, K., Tong, Z., Liu, X., Zhang, J., & Tong, S. (2020). Quantitative assessment and driving force analysis of vegetation drought risk to climate change:Methodology and application in Northeast China. *Agricultural and Forest Meteorology*, *282-283*, 107865. https://doi.org/10.1016/j.agrformet.2019.107865

Li, X., Li, Y., Chen, A., Gao, M., Slette, I. J., & Piao, S. (2019). The impact of the 2009/2010 drought on vegetation growth and terrestrial carbon balance in Southwest China. *Agricultural and Forest Meteorology*, *269*, 239-248. https://doi.org/10.1016/j.agrformet.2019.01.036

Li, X., Lu, H., Yu, L., & Yang, K. (2018). Comparison of the Spatial Characteristics of Four Remotely Sensed Leaf Area Index Products over China: Direct Validation and Relative Uncertainties. *Remote Sensing*, *10*(1), 148. https://doi.org/10.3390/rs10010148

Liang, S., Cheng, J., Jia, K., Jiang, B., Liu, Q., Xiao, Z., et al. (2021). The Global Land Surface Satellite (GLASS) Product Suite. *Bulletin of the American Meteorological Society*, *102*(2), E323-E337. https://doi.org/10.1175/BAMS-D-18-0341.1

Lin, A. L., Li, C. H., Gu, D. J., & Zheng, B. (2012). Variation and causes of persistent drought events in Guangdong province. *Journal of Tropical Meteorology*, *18*(1), 54-64. https://doi.org/10.3969/j.issn.1006-8775.2012.01.006

Liu, L., Jiang, T., & Yuan, F. (2009). Observed (1961-2007) and projected (2011-2060) climate change in the Pearl River Basin. Advances in Climate Change Research, 5(4), 209-214.

Liu, W., Zhan, J., Zhao, F., Wang, C., Zhang, F., Teng, Y., et al. (2022). Spatio-temporal variations of ecosystem services and their drivers in the Pearl River Delta, China. *Journal of Cleaner Production*, *337*, 130466. https://doi.org/10.1016/j.jclepro.2022.130466

Liu, W., Zhan, J., Zhao, F., Yan, H., Zhang, F., & Wei, X. (2019). Impacts of urbanization-induced land-use changes on ecosystem services: A case study of the Pearl River Delta Metropolitan Region, China. *Ecological Indicators*, *98*, 228-238. https://doi.org/10.1016/j.ecolind.2018.10.054

Liu, Y., You, M., Zhu, J., Wang, F., & Ran, R. (2019). Integrated risk assessment for agricultural drought and flood disasters based on entropy information diffusion theory in the middle and lower reaches of the Yangtze River, China. *International Journal of Disaster Risk Reduction*, *38*, 101194. https://doi.org/10.1016/j.ijdrr.2019.101194

Lu, H., Xue, J, & Guo, D. (2017). Efficacy of planting date adjustment as a cultivation strategy to cope with drought stress and increase rainfed maize yield and water-use efficiency. *Agricultural Water Management*, *179*, 227-235. https://doi.org/10.1016/j.agwat.2016.09.001

Madsen, H., & Rosbjerg, D. (1995). On the modelling of extreme droughts. *IAHS Publications-Series of Proceedings and Reports-Intern Assoc Hydrological Sciences*, *231*, 377-386.

Malhi, Y., Franklin, J., Seddon, N., Solan, M., Turner, M. G., Field, C. B., & Knowlton, N. (2020). Climate change and ecosystems: threats, opportunities and solutions. *Philosophical Transactions of the Royal Society B: Biological Sciences*, *375*(1794), 20190104. https://doi.org/10.1098/rstb.2019.0104

Marusig, D., Petruzzellis, F., Tomasella, M., Napolitano, R., Altobelli, A., & Nardini, A. (2020). Correlation of Field-Measured and Remotely Sensed Plant Water Status as a Tool to Monitor the Risk of Drought-Induced Forest Decline. *Forests*, *11*(1). https://doi.org/10.3390/f11010077

McKee, T. B., Doesken, N. J., & Kleist, J. (1993). The relationship of drought frequency and duration to time scales. *Proceedings of the 8th Conference on Applied Climatology,* American Meteorological Society, 179–183.

Mega, R., Abe, F., Kim, J.-S., Tsuboi, Y., Tanaka, K., Kobayashi, H., et al. (2019). Tuning water-use efficiency and drought tolerance in wheat using abscisic acid receptors. *Nature Plants*, *5*(2), 153-159. https://doi.org/10.1038/s41477-019-0361-8

Meisser, M., Vitra, A., Deléglise, C., Dubois, S., Probo, M., Mosimann, E., et al. (2019). Nutrient limitations induced by drought affect forage N and P differently in two permanent grasslands. *Agriculture, Ecosystems & Environment*, *280*, 85-94. https://doi.org/10.1016/j.agee.2019.04.027

Melchiorri, M., Florczyk, A. J., Freire, S., Schiavina, M., Pesaresi, M., & Kemper, T. (2018). Unveiling 25 Years of Planetary Urbanization with Remote Sensing: Perspectives from the Global Human Settlement Layer. *Remote Sensing*, *10*(5). https://doi.org/10.3390/rs10050768

Mesbahzadeh, T., Mirakbari, M., Mohseni Saravi, M., Soleimani Sardoo, F., & Miglietta, M. M. (2020). Meteorological drought analysis using copula theory and drought indicators under climate change scenarios (RCP). *Meteorological Applications*, *27*(1), e1856. https://doi.org/10.1002/met.1856

Meza, I., Siebert, S., Döll, P., Kusche, J., Herbert, C., Eyshi Rezaei, E., et al. (2020). Global-scale drought risk assessment for agricultural systems. *Nat. Hazards Earth Syst. Sci.*, *20*(2), 695-712. https://doi.org/10.5194/nhess-20-695-2020

Munns Jr, W. R., Rea, A. W., Suter II, G. W., Martin, L., Blake-Hedges, L., Crk, T., et al. (2016). Ecosystem services as assessment endpoints for ecological risk assessment. *Integrated Environmental Assessment and Management*, *12*(3), 522-528. https://doi.org/10.1002/ieam.1707

Myneni, R. B., Ramakrishna, R., Nemani, R., & Running, S. W. (1997). Estimation of global leaf area index and absorbed par using radiative transfer models. *IEEE Transactions on Geoscience and Remote Sensing*, *35*(6), 1380-1393. https://doi.org/10.1109/36.649788

Navarro-Cerrillo, R. M., Sánchez-Salguero, R., Rodriguez, C., Duque Lazo, J., Moreno-Rojas, J. M., Palacios-Rodriguez, G., & Camarero, J. J. (2019). Is thinning an alternative when trees could die in response to drought? The case of planted Pinus nigra and P. Sylvestris stands in southern Spain. *Forest Ecology and Management*, *433*, 313-324. https://doi.org/10.1016/j.foreco.2018.11.006

Nawaz, F., Shehzad, M. A., Majeed, S., Ahmad, K. S., Aqib, M., Usmani, M. M., & Shabbir, R. N. (2020). Role of Mineral Nutrition in Improving Drought and Salinity Tolerance in Field Crops. In M. Hasanuzzaman (Ed.), *Agronomic Crops: Volume 3: Stress Responses and Tolerance* (pp. 129-147). Springer Singapore.

https://doi.org/10.1007/978-981-15-0025-1_8

Noh, T. G., Yeh, S. W., Hyun, Y. K., & Hwang, S. O. (2021). Non-stationary characteristics of intraseasonal precipitation variability in Northeast Asia during the boreal summer. *International Journal of Climatology*, *41*(1), 714-725. https://doi.org/10.1002/joc.6647

Oikonomou, P. D., Tsesmelis, D. E., Waskom, R. M., Grigg, N. S., & Karavitis, C. A. (2019). Enhancing the standardized drought vulnerability index by integrating spatiotemporal information from satellite and in situ data. *Journal of Hydrology*, *569*, 265-277. https://doi.org/10.1016/j.jhydrol.2018.11.058

Orth, R., Destouni, G., Jung, M., & Reichstein, M. (2020). Large-scale biospheric drought response intensifies linearly with drought duration in arid regions. *Biogeosciences*, *17*(9), 2647-2656. https://doi.org/10.5194/bg-17-2647-2020

Peduzzi, P., Dao, H., Herold, C., & Mouton, F. (2009). Assessing global exposure and vulnerability towards natural hazards: the Disaster Risk Index. *Nat. Hazards Earth Syst. Sci.*, *9*(4), 1149-1159. https://doi.org/10.5194/nhess-9-1149-2009

Pescaroli, G., & Alexander, D. (2018). Understanding Compound, Interconnected, Interacting, and Cascading Risks: A Holistic Framework. *Risk Analysis*, *38*(11), 2245-2257. https://doi.org/10.1111/risa.13128

Peters, J. M. R., López, R., Nolf, M., Hutley, L. B., Wardlaw, T., Cernusak, L. A., & Choat, B. (2021). Living on the edge: A continental-scale assessment of forest vulnerability to drought. *Global Change Biology*, *27*(15), 3620-3641. https://doi.org/10.1111/gcb.15641

Phillips, C. A., Caldas, A., Cleetus, R., Dahl, K. A., Declet-Barreto, J., Licker, R., et al. (2020). Compound climate risks in the COVID-19 pandemic. *Nature Climate Change*, *10*(7), 586-588. https://doi.org/10.1038/s41558-020-0804-2

Quan, Q., Zhang, F., Tian, D., Zhou, Q., Wang, L., & Niu, S. (2018). Transpiration Dominates Ecosystem Water-Use Efficiency in Response to Warming in an Alpine Meadow. *Journal of Geophysical Research: Biogeosciences*, *123*(2), 453-462. https://doi.org/10.1002/2017JG004362

Quijano, J. A., Jaimes, M. A., Torres, M. A., Reinoso, E., Castellanos, L., Escamilla, J., & Ordaz, M. (2015). Event-based approach for probabilistic agricultural drought risk assessment under rainfed conditions. *Natural Hazards*, *76*(2), 1297-1318. https://doi.org/10.1007/s11069-014-1550-4

Rahimpour, V., Zeng, Y., Mannaerts, C. M., & Su, Z. (2016). Attributing seasonal variation of daily extreme precipitation events across The Netherlands. *Weather and Climate Extremes*, *14*, 56-66. https://doi.org/10.1016/j.wace.2016.11.003

Rao, C. A. R., Raju, B. M. K., Rao, A., Rao, K. V., Rao, V. U. M., Ramachandran, K., et al. (2016). A district level assessment of vulnerability of Indian agriculture to climate change. *Current Science*, *110*(10), 1939-1946. https://doi.org/10.18520/cs/v110/i10/1939-1946

Rasche, L., & Taylor, R. A. J. (2019). EPIC-GILSYM: Modelling crop-pest insect interactions and management with a novel coupled crop-insect model. *Journal of Applied Ecology*, *56*(8), 2045-2056. https://doi.org/10.1111/1365-2664.13426

Rashid, M. M., & Beecham, S. (2019). Development of a non-stationary Standardized Precipitation Index and its application to a South Australian climate. *Science of The Total Environment*, *657*, 882-892. https://doi.org/10.1016/j.scitotenv.2018.12.052

Ray, R. L., Fares, A., & Risch, E. (2018). Effects of Drought on Crop Production and Cropping Areas in Texas. *Agricultural & Environmental Letters*, *3*(1), 170037. https://doi.org/10.2134/ael2017.11.0037

Restaino, C., Young, D. J. N., Estes, B., Gross, S., Wuenschel, A., Meyer, M., & Safford, H. (2019). Forest structure and climate mediate drought-induced tree mortality in forests of the Sierra Nevada, USA. *Ecological Applications*, *29*(4), e01902. https://doi.org/10.1002/eap.1902

Rigby, R. A., & Stasinopoulos, D. M. (2005). Generalized additive models for location, scale and shape. *Journal of the Royal Statistical Society: Series C (Applied Statistics)*, *54*(3), 507-554. https://doi.org/10.1111/j.1467-9876.2005.00510.x

Rupp, D.E., Hawkins, L.R., Li, S., Koszuta, M. & Siler, N. (2022). Spatial patterns of extreme precipitation and their changes under~ 2° C global warming: a large-ensemble study of the western USA. *Climate Dynamics*, 59, 2363-2379. https://doi.org/10.1007/s00382-022-06214-3

Salas, J. D., Obeysekera, J., & Vogel, R. M. (2018). Techniques for assessing water infrastructure for nonstationary extreme events: a review. *Hydrological Sciences Journal*, *63*(3), 325-352. https://doi.org/10.1080/02626667.2018.1426858

Sarhadi, A., Burn, D. H., Concepción Ausín, M., & Wiper, M. P. (2016). Time-varying nonstationary multivariate risk analysis using a dynamic Bayesian copula.

Water Resources Research, *52*(3), 2327-2349. https://doi.org/10.1002/2015WR018525

Scheuer, S., Haase, D., Haase, A., Wolff, M., & Wellmann, T. (2021). A glimpse into the future of exposure and vulnerabilities in cities? Modelling of residential location choice of urban population with random forest. *Nat. Hazards Earth Syst. Sci.*, *21*(1), 203-217. https://doi.org/10.5194/nhess-21-203-2021

Schwarz, G. (1978). Estimating the Dimension of a Model. *The Annals of Statistics*, *6*(2), 461-464. http://www.jstor.org/stable/2958889

Sharafi, L., Zarafshani, K., Keshavarz, M., Azadi, H., & Van Passel, S. (2020). Drought risk assessment: Towards drought early warning system and sustainable environment in western Iran. *Ecological Indicators*, *114*, 106276. https://doi.org/10.1016/j.ecolind.2020.106276

Sillmann, J., Shepherd, T. G., van den Hurk, B., Hazeleger, W., Martius, O., Slingo, J., & Zscheischler, J. (2021). Event-Based Storylines to Address Climate Risk. *Earth's Future*, *9*(2), e2020EF001783. https://doi.org/10.1029/2020EF001783

Singh, C., Wang-Erlandsson, L., Fetzer, I., Rockström, J., & van der Ent, R. (2020). Rootzone storage capacity reveals drought coping strategies along rainforest-savanna transitions. *Environmental Research Letters*, *15*(12), 124021. https://doi.org/10.1088/1748-9326/abc377

Song, Y., Ma, M., & Veroustraete, F. (2010). Comparison and conversion of AVHRR GIMMS and SPOT VEGETATION NDVI data in China. *International Journal of Remote Sensing*, *31*(9), 2377-2392. https://doi.org/10.1080/01431160903002409

Spade, D., de Beurs, K., & Shafer, M. (2020). Major Over- and Underestimation of Drought Found in NOAA's Climate Divisional SPI Dataset. *Journal of Applied Meteorology and Climatology*, *59*(9), 1469-1480. https://doi.org/10.1175/JAMC-D-19-0272.1

Stasinopoulos, D. M., & Rigby, R. A. (2007). Generalized Additive Models for Location Scale and Shape (GAMLSS) in R. *Journal of Statistical Software*, *23*(7), 46. https://doi.org/10.18637/jss.v023.i07

Stocker, B. D., Zscheischler, J., Keenan, T. F., Prentice, I. C., Seneviratne, S. I., & Peñuelas, J. (2019). Drought impacts on terrestrial primary production underestimated by satellite monitoring. *Nature Geoscience*, *12*(4), 264-270. https://doi.org/10.1038/s41561-019-0318-6

Strzepek, K., Yohe, G., Neumann, J., & Boehlert, B. (2010). Characterizing changes in drought risk for the United States from climate change. *Environmental Research Letters*, *5*(4), 044012. https://doi.org/10.1088/1748-9326/5/4/044012

Suk, J. E., Vaughan, E. C., Cook, R. G., & Semenza, J. C. (2020). Natural disasters and infectious disease in Europe: a literature review to identify cascading risk pathways. *European Journal of Public Health*, *30*(5), 928-935. https://doi.org/10.1093/eurpub/ckz111

Svensson, C., Hannaford, J., & Prosdocimi, I. (2017). Statistical distributions for monthly aggregations of precipitation and streamflow in drought indicator applications. *Water Resources Research*, *53*(2), 999-1018. https://doi.org/10.1002/2016WR019276

Swinton, S. M., Lupi, F., Robertson, G. P., & Hamilton, S. K. (2007). Ecosystem services and agriculture: Cultivating agricultural ecosystems for diverse benefits. *Ecological Economics*, *64*(2), 245-252. https://doi.org/10.1016/j.ecolecon.2007.09.020

Taghvaeian, S., Neale Christopher, M. U., Osterberg John, C., Sritharan Subramania, I., & Watts Doyle, R. (2018). Remote Sensing and GIS Techniques for Assessing Irrigation Performance: Case Study in Southern California. *Journal of Irrigation and Drainage Engineering*, *144*(6), 05018002. https://doi.org/10.1061/(ASCE)IR.1943-4774.0001306

Teixeira, A. H. d. C. (2010). Determining Regional Actual Evapotranspiration of Irrigated Crops and Natural Vegetation in the São Francisco River Basin (Brazil) Using Remote Sensing and Penman-Monteith Equation. *Remote Sensing*, *2*(5). https://doi.org/10.3390/rs0251287

Teutschbein, C., Jonsson, E., Todorović, A., Tootoonchi, F., Stenfors, E., & Grabs, T. (2022). Future Drought Propagation through the Water-Energy-Food-Ecosystem Nexus–a Nordic Perspective. *Journal of Hydrology*, 128963. https://doi.org/10.1016/j.jhydrol.2022.128963

Tirivarombo, S., Osupile, D., & Eliasson, P. (2018). Drought monitoring and analysis: Standardised Precipitation Evapotranspiration Index (SPEI) and Standardised Precipitation Index (SPI). *Physics and Chemistry of the Earth, Parts A/B/C*, 106, 1-10. https://doi.org/https://doi.org/10.1016/j.pce.2018.07.001

Trenberth, K. E., Dai, A., van der Schrier, G., Jones, P. D., Barichivich, J., Briffa, K. R., & Sheffield, J. (2014). Global warming and changes in drought. *Nature Climate*

Change, *4*(1), 17-22. https://doi.org/10.1038/nclimate2067

Tsakiris, G. (2017). Drought Risk Assessment and Management. *Water Resources Management*, *31*(10), 3083-3095. https://doi.org/10.1007/s11269-017-1698-2

UNISDR. (2015). *Sendai framework for disaster risk reduction 2015–2030*. https://www.preventionweb.net/files/43291_sendaiframeworkfordrren.pdf

Vasiliades, L., Galiatsatou, P., & Loukas, A. (2015). Nonstationary Frequency Analysis of Annual Maximum Rainfall Using Climate Covariates. *Water Resources Management*, *29*(2), 339-358. https://doi.org/10.1007/s11269-014-0761-5

Vicente-Serrano, S. M., Beguería, S., & López-Moreno, J. I. (2010). A Multiscalar Drought Index Sensitive to Global Warming: The Standardized Precipitation Evapotranspiration Index. *Journal of Climate*, *23*(7), 1696-1718. https://doi.org/10.1175/2009JCLI2909.1

Villarini, G., Serinaldi, F., Smith, J. A., & Krajewski, W. F. (2009). On the stationarity of annual flood peaks in the continental United States during the 20th century. *Water Resources Research*, *45*(8). https://doi.org/10.1029/2008WR007645

Villarini, G., Smith, J. A., Serinaldi, F., Bales, J., Bates, P. D., & Krajewski, W. F. (2009). Flood frequency analysis for nonstationary annual peak records in an urban drainage basin. *Advances in Water Resources*, *32*(8), 1255-1266. https://doi.org/10.1016/j.advwatres.2009.05.003

Vinnarasi, R., & Dhanya, C. T. (2019). Bringing realism into a dynamic copula-based non-stationary intensity-duration model. *Advances in Water Resources*, *130*, 325-338. https://doi.org/10.1016/j.advwatres.2019.06.009

Wamsler, C., Niven, L., Beery, T. H., Bramryd, T., Ekelund, N., Jönsson, K. I., et al. (2016). Operationalizing ecosystem-based adaptation: harnessing ecosystem services to buffer communities against climate change. *Ecology and Society*, *21*(1), Article 31. https://doi.org/10.5751/ES-08266-210131

Wang, H., Duan, K., Liu, B., & Chen, X. (2021). Assessing the large-scale plant–water relations in the humid, subtropical Pearl River basin of China. *Hydrol. Earth Syst. Sci.*, *25*(9), 4741-4758. https://doi.org/10.5194/hess-25-4741-2021

Wang, J., Wang, K., Zhang, M., & Zhang, C. (2015). Impacts of climate change and human activities on vegetation cover in hilly southern China. *Ecological Engineering*, *81*, 451-461. https://doi.org/10.1016/j.ecoleng.2015.04.022

Wang, Y., Duan, L., Liu, T., Li, J., & Feng, P. (2020). A Non-stationary Standardized Streamflow Index for hydrological drought using climate and human-induced indices as covariates. *Science of The Total Environment*, *699*, 134278. https://doi.org/https://doi.org/10.1016/j.scitotenv.2019.134278

Wang, Y., Li, J., Feng, P., & Hu, R. (2015). A Time-Dependent Drought Index for Non-Stationary Precipitation Series. *Water Resources Management*, *29*(15), 5631-5647. https://doi.org/10.1007/s11269-015-1138-0

Wens, M., Johnson, J. M., Zagaria, C., & Veldkamp, T. I. E. (2019). Integrating human behavior dynamics into drought risk assessment—A sociohydrologic, agent-based approach. *WIREs Water*, *6*(4), e1345. https://doi.org/10.1002/wat2.1345

Weraduwage, S. M., Chen, J., Anozie, F. C., Morales, A., Weise, S. E., & Sharkey, T. D. (2015). The relationship between leaf area growth and biomass accumulation in Arabidopsis thaliana. *Frontiers in Plant Science*, *6*, 167. https://doi.org/10.3389/fpls.2015.00167

Xiong, L., Jiang, C., Xu, C., Yu, K., & Guo, S. (2015). A framework of change-point detection for multivariate hydrological series. *Water Resources Research*, *51*(10), 8198-8217. https://doi.org/10.1002/2015WR017677

Yang, G., Pu, R., Zhang, J., Zhao, C., Feng, H., & Wang, J. (2013). Remote sensing of seasonal variability of fractional vegetation cover and its object-based spatial pattern analysis over mountain areas. *ISPRS Journal of Photogrammetry and Remote Sensing*, *77*, 79-93. https://doi.org/10.1016/j.isprsjprs.2012.11.008

Yang, L., Du, Y., Wang, D., Wang, C., & Wang, X. (2015). Impact of intraseasonal oscillation on the tropical cyclone track in the South China Sea. *Climate Dynamics*, *44*(5), 1505-1519. https://doi.org/10.1007/s00382-014-2180-y

Yang, Y., Roderick, M. L., Yang, D., Wang, Z., Ruan, F., McVicar, T. R., et al. (2021). Streamflow stationarity in a changing world. *Environmental Research Letters*, *16*(6), 064096. https://doi.org/10.1088/1748-9326/ac08c1

Yuan, W., Zheng, Y., Piao, S., Ciais, P., Lombardozzi, D., Wang, Y., et al. (2019). Increased atmospheric vapor pressure deficit reduces global vegetation growth. *Science Advances*, *5*(8), eaax1396. https://doi.org/10.1126/sciadv.aax1396

Zhang, F., Chen, Y., Zhang, J., Guo, E., Wang, R., & Li, D. (2019). Dynamic drought risk assessment for maize based on crop simulation model and multi-source drought indices. *Journal of Cleaner Production*, *233*, 100-114. https://doi.org/10.1016/j.jclepro.2019.06.051

Zhang, G., Ganguly, S., Nemani, R. R., White, M. A., Milesi, C., Hashimoto, H., et al. (2014). Estimation of forest aboveground biomass in California using canopy height and leaf area index estimated from satellite data. *Remote Sensing of Environment*, *151*, 44-56. https://doi.org/10.1016/j.rse.2014.01.025

Zhang, H., Qin, J., & Li, Y. (2011). Climatic background of cold and wet winter in southern China: part I observational analysis. *Climate Dynamics*, *37*(11), 2335-2354. https://doi.org/10.1007/s00382-011-1022-4

Zhang, L., Zhu, X., Fraedrich, K., Sielmann, F., & Zhi, X. (2014). Interdecadal variability of winter precipitation in Southeast China. *Climate Dynamics*, *43*(7), 2239-2248. https://doi.org/10.1007/s00382-014-2048-1

Zhang, T., Zhou, J., Yu, P., Li, J., Kang, Y., & Zhang, B. (2023). Response of ecosystem gross primary productivity to drought in northern China based on multi-source remote sensing data. *Journal of Hydrology*, 616, 128808. https://doi.org/10.1016/j.jhydrol.2022.128808

Zhang, X., Li, X., Manzanedo, R. D., D'Orangeville, L., Lv, P., Wang, C., et al. (2021). High risk of growth cessation of planted larch under extreme drought. *Environmental Research Letters*, *16*(1), 014040. https://doi.org/10.1088/1748-9326/abd214

Zhang, Y., & Ye, A. (2020). Spatial and temporal variations in vegetation coverage observed using AVHRR GIMMS and Terra MODIS data in the mainland of China. *International Journal of Remote Sensing*, *41*(11), 4238-4268. https://doi.org/10.1080/01431161.2020.1714781

Zhao, W., Deng, C., & Ngo, C. (2018). k-means: A revisit. *Neurocomputing*, *291*, 195-206. https://doi.org/10.1016/j.neucom.2018.02.072

Zheng, Y., Shen, R., Wang, Y., Li, X., Liu, S., Liang, S., et al. (2020). Improved estimate of global gross primary production for reproducing its long-term variation, 1982–2017. *Earth Syst. Sci. Data*, *12*(4), 2725-2746. https://doi.org/10.5194/essd-12-2725-2020

Appendix A. Supplementary data

Supplementary data for

Assessment of dynamic drought-induced ecosystem risk: integrating time-varying hazard frequency, exposure and vulnerability

Contents of this file

Text S1. Method for pooling interdependent droughts and excluding minor droughts

Two successive droughts are assumed to be inter-dependent and subsequently merged into a single one with attributes updated using Eq. (S1) if two prerequisites are both satisfied which are that (a) adjacent droughts occur less than a user-specified inter-event time t_c and (b) the ratio between the inter-event excess volume v_{i+2} colored in green in Fig. 3 and the previous drought severity S_{i+2} is below a predefined threshold ρ_c. In addition to pooling dependent droughts, minor droughts are likely to distort the extreme value modeling (Fleig et al., 2006). Therefore, minor droughts with duration or severity (Case 1 in Fig. 3) lower than the designated percentage (r_d and r_s) of mean duration and severity are removed from analysis (see Eq. (S2)) to minimize potential bias in the derived drought frequency. According to the outcome of sensitivity analysis conducted by Tu et al. (2019) in the PRB and a relevant study by Van Loon and Van Lanen (2012), appropriate values of t_c, ρ_c, r_d and r_s are set to be 10 days, 0.2, 0.41 and 0.41 in the current study, respectively.

$$\begin{cases} D_{pooled} = D_i + t_i + D_{i+1}, \\ S_{pooled} = S_i - v_i + S_{i+1}, \end{cases} \quad \text{if } t < t_c \text{ and } v_i / S_i < \rho_c \tag{S1}$$

$$\begin{cases} D_{excluded} = 0, \\ S_{excluded} = 0, \end{cases} \quad \text{if } D_i / \bar{D} < r_d \text{ or } S_i / \bar{S} < r_s \tag{S2}$$

where $\{D_i, S_i\}$ and $\{D_{i+1}, S_{i+1}\}$ symbolize the pairwise duration and severity of two consecutive droughts, and attributes of the pooled and excluded droughts are denoted by D and S with subscripts $pooled$ and $excluded$, respectively.

References

Fleig, A. K., Tallaksen, L. M., Hisdal, H., & Demuth, S. (2006). A global evaluation of streamflow drought characteristics. *Hydrol. Earth Syst. Sci.*, *10*(4), 535-552. https://doi.org/10.5194/hess-10-535-2006

Tu, X., Du, Y., Singh Vijay, P., Chen, X., Zhao, Y., Ma, M., et al. (2019). Bivariate Design of Hydrological Droughts and Their Alterations under a Changing Environment. Journal of Hydrologic Engineering, 24(6), 04019015. https://doi.org/10.1061/(ASCE)HE.1943-5584.0001788

Van Loon, A. F., & Van Lanen, H. A. J. (2012). A process-based typology of hydrological drought. Hydrol. Earth Syst. Sci., 16(7), 1915-1946. https://doi.org/10.5194/hess-16-1915-2012

Text S2. The copula likelihood ratio-based (CLR) test for detecting nonstationarity in duration-severity dependence structure

A pairwise duration-severity series under investigation $\{\mathbf{y}_1, \ldots, \mathbf{y}_n\} = \{(D_1, S_1), \ldots, (D_n, S_n)\}$ is assumed to follow a multivariate distribution $F\left(\mathbf{y}_i \middle| \theta_i^c\right)$. For the best-fitted copula, the null hypothesis H_0 of no changepoint in dependence strength is shown by Eq. (S3), in which the copula parameters are all the same. The alternative hypothesis H_1 is that there is a notable change in copula parameters at a time k, which implies the existence of temporal variation in dependence strength.

$$\begin{cases} H_0: \quad \theta_1^c = \theta_2^c = \ldots = \theta_n^c = \eta_0 \\ H_1: \quad \theta_1^c = \ldots = \theta_k^c = \eta_1, \ \theta_{k+1}^c = \ldots = \theta_n^c = \eta_2, \text{ and } \eta_1 \neq \eta_2 \end{cases} \tag{S3}$$

Subsequently, the CLR test statistic Z_n (Eq. (S4)) is formulated by calculating the maximum likelihood ratio in the logarithmic form, to determine whether to accept the null hypothesis or not.

$$\begin{cases} Z_n = \max\limits_{1 \le k \le n-1} \left[-2\ln\left(\Lambda_k\right)\right] \\ \Lambda_k = \dfrac{L_n\left(\hat{\eta}_0\right)}{L_k\left(\hat{\eta}_1\right)L_{n-k}\left(\hat{\eta}_2\right)} = \dfrac{\prod\limits_{i=1}^{n} c\left(\mathbf{u}_i \middle| \hat{\eta}_0\right)}{\prod\limits_{i=1}^{k} c\left(\mathbf{u}_i \middle| \hat{\eta}_1\right) \prod\limits_{i=k+1}^{n} c\left(\mathbf{u}_i \middle| \hat{\eta}_2\right)} \end{cases} \tag{S4}$$

where $L_n(\,)$ is the likelihood for the whole series of pairwise duration and severity, $L_k(\,)$ and $L_{n-k}(\,)$ are symbols of the likelihood before or after time k, $\hat{\eta}_0$, $\hat{\eta}_1$ and $\hat{\eta}_2$ represent the estimated copula parameters, $\mathbf{u}$ is a vector composed of cumulative probability of duration and severity, and $c(\,)$ denotes a copula density function.

If the statistic Z_n is greater than the critical value computed using Eq. (S5), the null hypothesis will be rejected at the 5% significance level and k is identified as a changepoint in dependence structure. The existence of changepoints notifies nonstationarity in duration-severity dependence. Otherwise, the stationary assumption regarding dependence structure is justified.

$$\begin{cases} P\left(Z_n^{1/2} \geq z\right) = \dfrac{z^p \exp\left(-z^2/2\right)}{2^{p/2}\Gamma\left(p/2\right)}\left[\ln\dfrac{(1-h)(1-l)}{hl} - \dfrac{p}{z^2}\ln\dfrac{(1-h)(1-l)}{hl} + \dfrac{4}{z^2} + \mathrm{O}\left(\dfrac{1}{z^2}\right)\right] \\ h = l = \left[\ln(n)\right]^{3/2} \big/ n \end{cases} \quad \text{(S5)}$$

in which p indicates the number of copula parameters, and n is the sample size.